LATERAL SPREADING OF SLOPES
Data report on tests SKH-5-12

S.K. Haigh[1]

CUED/D-SOILS/TR317 (2002)

[1] Research Associate, Cambridge University Engineering Department

Table of Contents

List of Figures

List of Tables

1. Introduction

The many large earthquakes of recent years, including those at Northridge (1994), Kobe (1995), Turkey (1999), Taiwan (1999) and Gujarat (2001) have shown the capacity of these large-magnitude events to cause massive damage to infrastructure and enormous loss of life. The concentrations of population in seismically active regions of the world, including the Pacific Rim, California and northern India has put many millions of people at risk when these large earthquakes strike. Whilst nothing can be done to prevent these earthquakes from occurring, efforts must be made to find ways to minimise the impact of these earthquakes on the population and infrastructure.

In many of these major earthquakes, large-scale damage due to liquefaction and especially due to the lateral spreading of liquefiable slopes has been observed. In the Niigata Earthquake of 1964, lateral spreading of up to 5 m was observed along the Shinano River (Hamada 1992). These large magnitude deformations have been shown to have devastating effects on structures founded on these slopes and lifelines passing over or through them.

This research was hence undertaken to investigate the lateral spreading of liquefiable slopes and to develop experimental techniques to be used in order to study the interaction of these spreading slopes with pile foundations. The research consisted of a series of eight beam centrifuge tests (SKH-5 to 12) two of which (SKH-6 & 7) were unsuccessful due to failure to achieve saturation and will hence not be discussed further. Full details of the analysis of these test results is given by Haigh (2002).

2. Experimental Procedure

The test series consisted of seven oil-saturated tests (SKH-5 to 11) and one dry test (SKH-12) carried out as a control. The models were all prepared and tested following the procedure outlined in the next section, with the exception of the dry model, in which the procedures for model saturation were obviously not required.

2.1 Model Preparation

All tests from SKH-5 through to SKH-12 comprised of slopes of loose liquefiable fraction E silica sand with properties as shown in Table 1 and particle size distribution as shown in Figure 1. The models were prepared to a nominal void ratio of 0.8 or an R_D (relative density) of 50% by air pluviation from an overhead hopper. Density was controlled by adjusting both the height of the hopper and the rate of pouring. End reservoirs of Fraction B silica sand, with properties as shown in Table 2 and particle size distribution as shown in Figure 1, were provided at the top and bottom of the slope to ensure a plane strain seepage condition through the model. These are separated from the rest of the sand by stainless steel mesh and are filled at the same rate as the rest of the model.

Table 1: Properties of fraction E silica sand. (after Tan, 1990)

Property	Value
ϕ_{crit}	32^0
D_{10}	0.095 mm
D_{50}	0.14 mm
D_{60}	0.15 mm
e_{min}	0.613
e_{max}	1.014
k with water at e = 0.72	0.98E-04 m/s
G_s	2.65

Table 2: Properties of fraction B silica sand. (after Lee, 1990)

Property	Value
ϕ_{crit}	36^0
D_{10}	0.84 mm
D_{50}	0.9 mm
D_{90}	1.07 mm
e_{min}	0.495
e_{max}	0.82
G_s	2.65

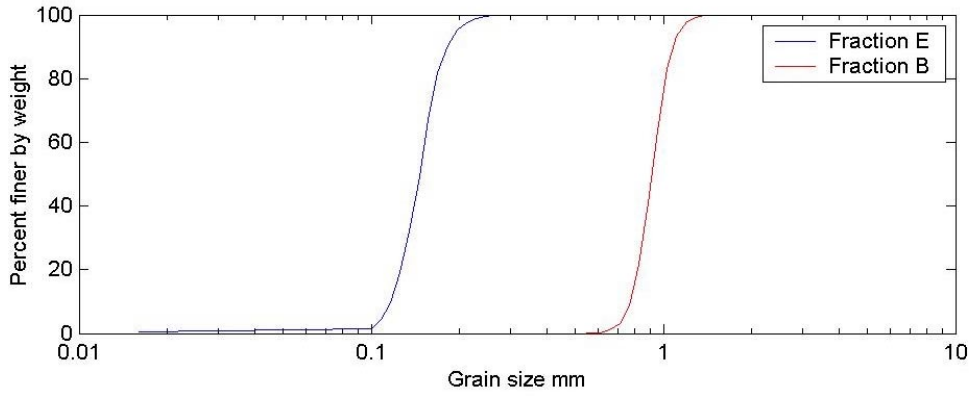

Figure 1: Particle size distributions for fraction E and fraction B silica sands.

Once sand has been poured to the final level, a lid is bolted to the top of the ESB box, with pump grease being applied to the joint to achieve a seal. A vacuum of greater than 95 kPa is then applied to the box to remove trapped air from the pore spaces. This ensures even saturation of the model as the silicone oil does not need to displace air from the pores and also increases the speed of seepage due to the enhanced pressure gradient between the oil reservoir and the model container. This does however introduce problems of sand boiling if oil is admitted at too great a speed. Silicone oil is then admitted to the base of the model through feed pipes fitted with needle valves to control flow-rate. A flow rate of 0.5 $kghr^{-1}$ per feed pipe was found to be sufficiently low to prevent piping of the model whilst still allowing saturation to be achieved in approximately 10 hours. The feed pipes are located in the reservoirs at top and bottom of the slope and consist of 8 mm diameter pipe with holes drilled at intervals to spread the oil across the model.

2.2 Test Procedure

After model preparation was complete, the SAM actuator and counterweight were loaded onto the centrifuge arm. The SAM was placed on a wooden block to make it hang level. The ESB box and shaking table were then ballasted with weights to make them hang horizontally from the crane and were lowered into place on the SAM. The SAM and ESB box were loaded separately onto the centrifuge in order to minimise model disturbance, as the oil-saturated slope is fairly unstable at 1 g.

Once the ESB box was in place on the SAM, wires from the instruments present in the model were connected to the junction boxes on the SAM and cable-tied into place.

After pre-flight checks had taken place, including such items as checking that enough pressure was available in the accumulator to fire earthquakes, the centrifuge was started and accelerated to 8g at which point both swinging platforms should have sat back against the end of the centrifuge arm. This was monitored by pairs of micro-switches at either end of the arm which are closed by the swing sitting against the end of the beam. The centrifuge speed at which this should occur for each swing

was calculated in the balance calculations and was compared with observed values as a safety check. In general (with SAM packages) the blue-end swing (SAM and ESB) swings up at 30 rpm and the red-end swing (counterweight) at 40 rpm.

Once both swings have swung up, the centrifuge was accelerated in stages to the required speed, in the case of the work described here 106 rpm or 50 g. Pore pressures were monitored during this acceleration stage in order to check the integrity of the package. When 50 g was reached, pumping commenced, with oil being admitted to the reservoir at the top of the slope and the sump being kept empty. Pore pressures within the model were monitored and oil was continuously admitted until a steady-state seepage regime was achieved with the water-table close to the surface of the slope.

When this condition was achieved, the model was ready to be subjected to an earthquake. Three-phase power was turned on to the SAM actuator and an offset was driven, changing the lever-arm length joining the package to the SAM. This was monitored by an LVDT (linearly variable displacement transducer) allowing a predictable earthquake magnitude to be achieved. Once this had been carried out, the compressed air supply to the clutch centring mechanism was turned on, forcing the clutch into a central position. The timer controlling the solid-state relays on the SAM package was then started, giving a ten second delay and then firing the earthquake. The timer also starts the data-acquisition system, which collects data during the earthquake and for a period afterwards.

After data-acquisition was complete, the data was uploaded from the CDAQS box and the decision was taken as to whether or not to fire subsequent earthquakes. If no further earthquakes were to be fired, the centrifuge was slowed and stopped. The SAM was then blocked up to hang level and the model was examined, measured and photographed.

3. Instrumentation

The models tested were instrumented with Birchall A23 accelerometers (ACC's) and Druck PDCR81 pore pressure transducers (PPT's) arranged throughout the sand of the model. Schematic instrumentation layouts for the centrifuge tests together with the coordinates of the instruments are shown in Figures 2 to 7 and Tables 3 to 8 respectively. The coordinate system used is x being the downslope coordinate from an origin at the end of the box, z being a vertical coordinate from the base of the ESB box and y the transverse coordinate from the edge of the box.

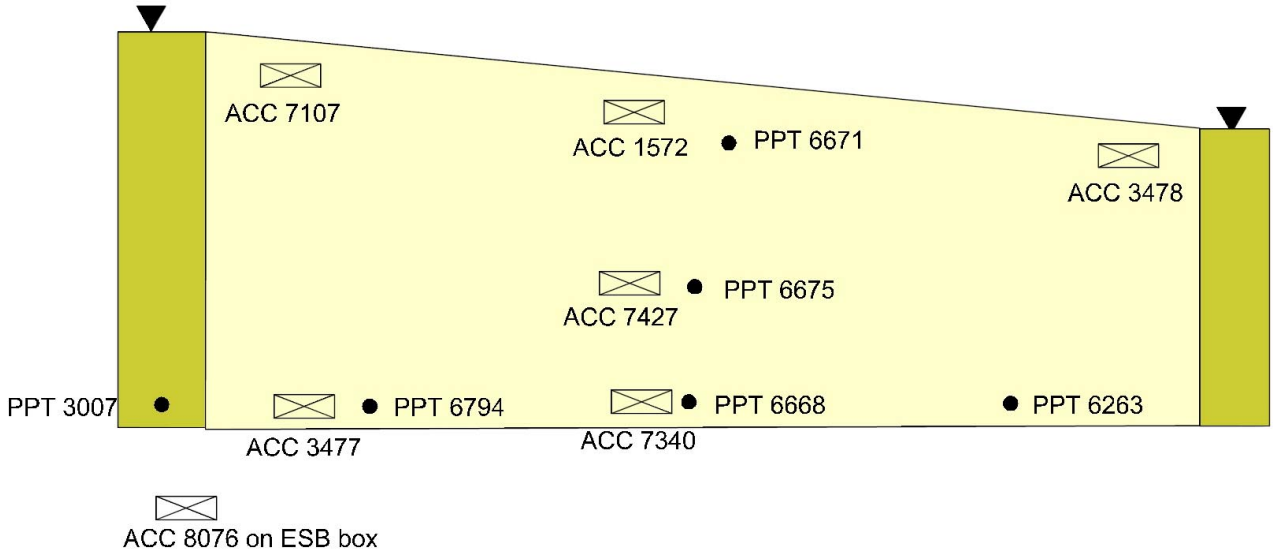

Figure 2: Instrument layout for test SKH-5

Table 3: Instrumentation coordinates for test SKH-5

Instrument	x (mm)	y (mm)	z (mm)
ACC1572	310	115	45
ACC3477	460	115	3
ACC3478	130	125	35
ACC7107	465	120	30
ACC7340	285	115	10
ACC7427	310	95	15
ACC8076	ESB box bottom ring		
PPT6263	110	95	5
PPT6668	280	115	3
PPT6671	280	120	30
PPT6675	280	115	20
PPT6794	445	115	3

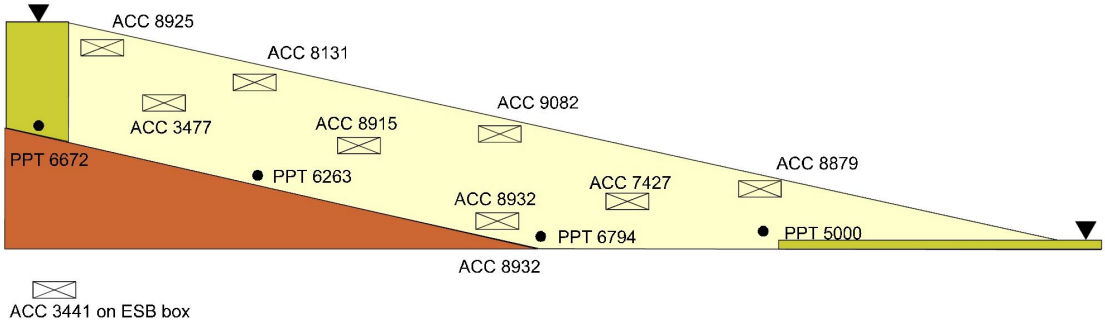

Figure 3: Instrument layout for test SKH-8

Table 4: Instrumentation coordinates for test SKH-8

Instrument	x (mm)	y (mm)	z (mm)
ACC3441	ESB box base ring		
ACC3477	420	110	70
ACC7427	200	125	50
ACC8131	320	170	75
ACC8879	130	115	50
ACC8915	330	160	60
ACC8925	445	145	90
ACC8932	250	155	40
ACC9082	220	14	65
PPT5000	175	90	35
PPT6263	380	110	50
PPT6794	255	75	40

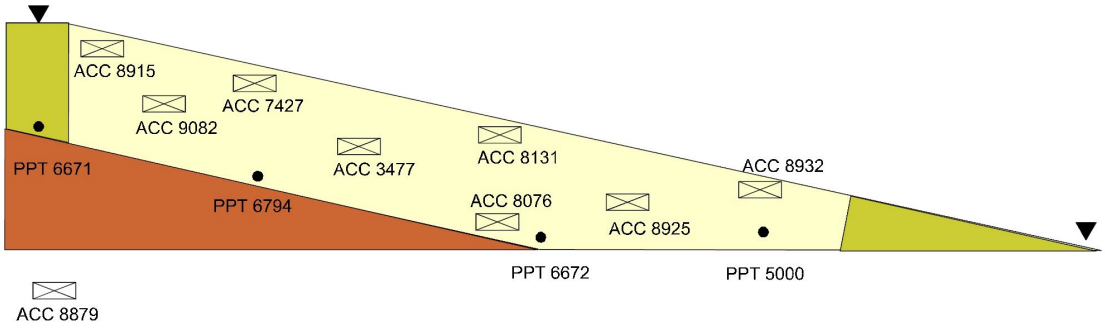

Figure 4: Instrument layout for test SKH-9

Table 5: Instrumentation coordinates for test SKH-9

Instrument	x (mm)	y (mm)	z (mm)
ACC3477	290	105	70
ACC7427	375	140	80
ACC8076	290	150	50
ACC8131	280	170	70
ACC8879	ESB box bottom ring		
ACC8915	470	160	100
ACC8925	180	150	60
ACC8932	145	100	45
ACC9082	370	140	80
PPT5000	180	105	35
PPT6672	325	90	50
PPT6794	420	115	75

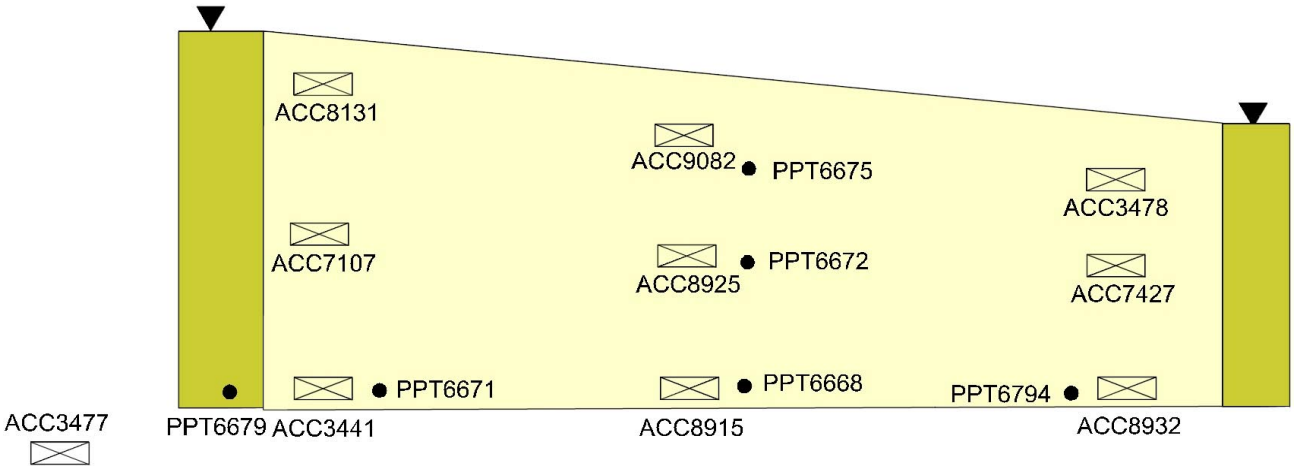

Figure 5: Instrument layout for test SKH-10

Table 6: Instrumentation coordinates for test SKH-10

Instrument	x (mm)	y (mm)	z (mm)
ACC3441	115	75	10
ACC3477	ESB box bottom ring		
ACC3478	465	75	50
ACC7107	105	75	40
ACC7427	475	100	20
ACC8131	140	90	90
ACC8915	240	75	10
ACC8925	305	100	30
ACC8932	470	80	0
ACC9082	305	110	60
PPT6668	270	130	0
PPT6672	320	130	30
PPT6675	320	140	60
PPT6794	440	110	0

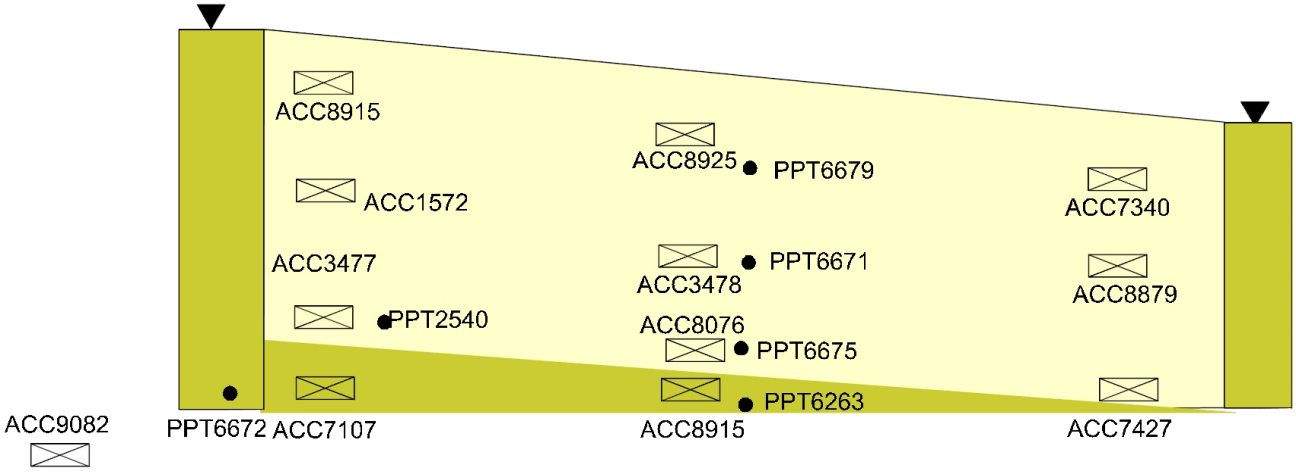

Figure 6: Instrument layout for test SKH-11

Table 7: Instrumentation coordinates for test SKH-11

Instrument	x (mm)	y (mm)	z (mm)
ACC1572	150	145	90
ACC3477	140	110	40
ACC3478	330	165	75
ACC7107	130	95	10
ACC7340	420	155	85
ACC7427	455	160	20
ACC8076	345	160	25
ACC8879	440	160	65
ACC8915	125	110	110
ACC8925	330	160	100
ACC8932	340	60	5
ACC9082	ESB bottom ring		
PPT2540	220	150	30
PPT6263	310	150	0
PPT6671	315	120	70
PPT6672	0	0	0
PPT6675	350	130	25
PPT6679	310	100	100

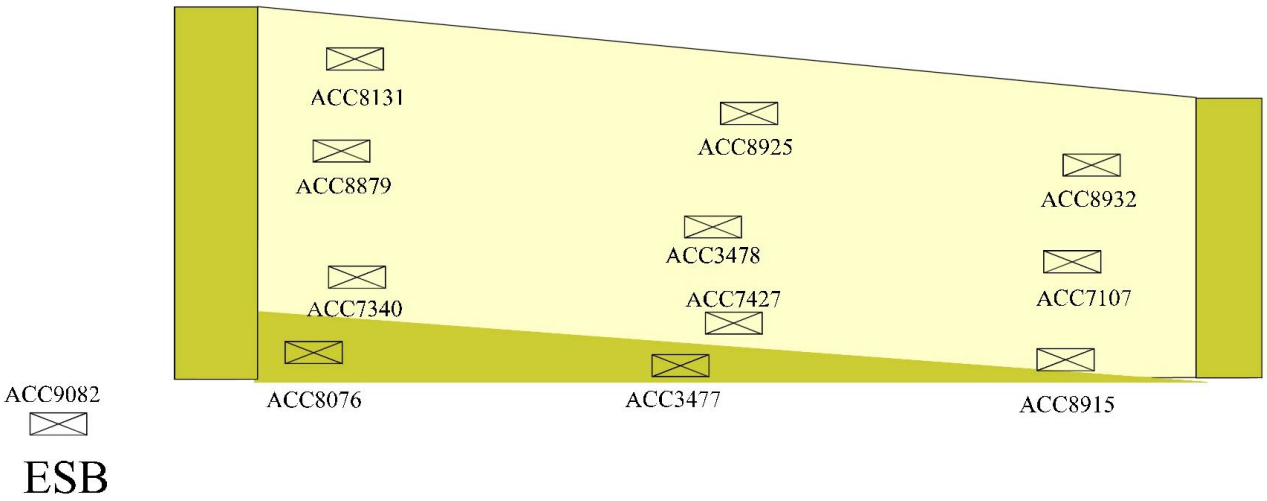

Figure 7: Instrument layout for test SKH-12

Table 8: Instrumentation coordinates for test SKH-12

Instrument	x (mm)	y (mm)	z (mm)
ACC3477	265	120	5
ACC3478	290	130	60
ACC7107	460	110	40
ACC7340	120	125	40
ACC7427	300	115	30
ACC8076	80	115	10
ACC8131	120	100	110
ACC8879	110	100	70
ACC8915	425	135	20
ACC8925	330	100	90
ACC8932	480	120	70
ACC9082	ESB bottom ring		

4. Results

Time-histories of acceleration and pore-pressure for the centrifuge tests are shown in Figures 8 through 27. Only a brief discussion of the results will be made here, further discussion can be found in Haigh (2002).

4.1 Test SKH-5

This model was subjected to two earthquakes of approximately 15% magnitude. The final measured ground displacement was 20 mm (1 m at prototype scale). From in-flight video, this was seen to have been accrued almost entirely during the first earthquake.

4.1.1 Earthquake 1

The results of test SKH-5 earthquake 1 are plotted in Figures 8 & 9. The data acquisition system crashed after 0.5 s, so the data for the end of the earthquake is not available. It can however be seen that the model was subjected to a 15% earthquake of 0.5 s duration. Pore-pressures consistent with full liquefaction built up over approximately four earthquake cycles.

4.1.2 Earthquake 2

The results of test SKH-5 earthquake 2 are plotted in Figures 10 & 11. This was a 20% magnitude earthquake of 0.5 s duration. Pore-pressures consistent with full liquefaction were seen to be achieved after approximately two earthquake cycles.

4.1.3 Earthquake 3

The results of test SKH-5 earthquake 3 are plotted in Figures 12 & 13. This was a 17% magnitude earthquake of 0.5 s duration. Pore-pressures consistent with full liquefaction built up over approximately three earthquake cycles.

4.2 Test SKH-8

This model was subjected to two earthquakes of approximately 20% magnitude. The final measured ground displacement was 12 mm (0.6 m at prototype scale).

4.2.1 Earthquake 1

The results of test SKH-8 earthquake 1 are plotted in Figures 14 & 15. This was a 25% magnitude earthquake of 0.5 s duration. Pore-pressures consistent with full liquefaction were seen to be achieved after approximately two earthquake cycles with rapid drainage being seen both during the earthquake and afterwards relative to the other tests discussed here. This is due to the relative thinness of the liquefiable layer in this test. Examination of accelerations recorded close to the head of the slope (ACC's 3477 & 8925) shows the higher harmonics of the earthquake being severely

attenuated resulting in near sinusoidal accelerations being measured after 0.3 s. This is explained in terms of inter-particle sliding by Haigh (2002).

4.2.2 Earthquake 2

The results of test SKH-8 earthquake 2 are plotted in Figures 16 & 17. This was a 26% magnitude earthquake of 0.9 s duration. Pore-pressures consistent with full liquefaction were seen to be achieved after approximately three earthquake cycles. The accelerations measured at the head of the slope again show the filtering of higher harmonics of the motion by sliding and become very asymmetric, peak positive (upslope) accelerations being three times those measured in the negative direction for ACC8925.

4.3 Test SKH-9

This model was subjected to one earthquake of approximately 15% magnitude. The final measured surface ground displacement was found to be approximately 15 mm (0.75 m at prototype scale). Marker lines at depth revealed that sub-surface deformations of 25 mm (1.25 m) were occurring at 20 mm (1 m) depth. This could be a feature of the rotation of surficial soil due to g-field curvature or due to toe restraint. This is further discussed by Haigh et al. (2000).

The results of test SKH-9 are plotted in Figures 18 & 19. The same filtering of higher harmonics as was seen in test SKH-8 can be seen from ACC3477.

4.4 Test SKH-10

This model was subjected to one earthquake of approximately 22% magnitude. The final measured surface ground displacement was found to be approximately 26 mm (1.3 m at prototype scale), though subsurface peak displacements were measured as up to 60 mm (3 m).

The results of test SKH-10 are plotted in Figures 20 & 21. Some filtering of higher harmonics can be seen from ACC7427. Unfortunately the data acquisition system crashed after 0.5 s, so later acceleration information is not available.

4.5 Test SKH-11

This model was subjected to one earthquake of approximately 20% magnitude. The final measured ground displacement was found to be approximately 28 mm (1.4 m at prototype scale).

The results of test SKH-11 are plotted in Figures 22 & 23. Looking at the response of ACC8076 at the end of the earthquake reveals different behaviour on odd and even cycles. This is revealed in FFT's as a component at 25 Hz, half of the earthquake frequency. This has been explained as being a feature of the natural frequency of the liquefied soil column, which was calculated based on shear wave velocities to be approximately 23 Hz by Haigh (2002).

4.6 Test SKH-12

This dry test was carried out as a control in order to highlight the importance of liquefaction to the displacements and dynamic behaviour of these slopes. This model was subjected to one earthquake of approximately 20% magnitude. No significant ground displacement was measured.

The results of test SKH-12 are plotted in Figure 24. Almost identical accelerations were measured at all instrument locations, highlighting that the base accelerations necessary to fail these shallow slopes in the absence of liquefaction are very high.

798 data points plotted per complete transducer record

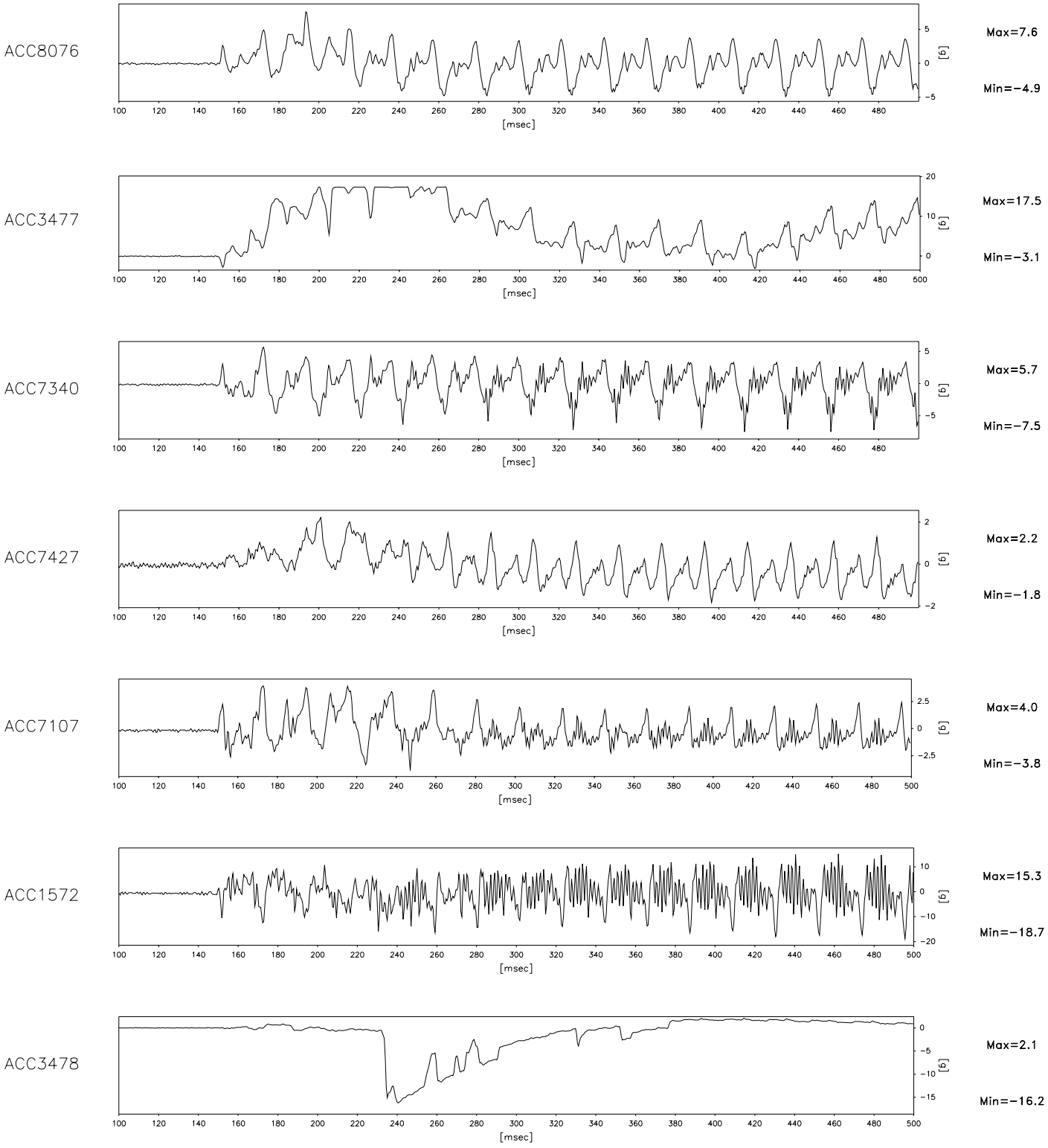

Scales : Model

TEST SKH−5 MODEL 3 deg slope FLIGHT 1		Short−Term TIME RECORDS	Earthquake 1	FIG.NO.

798 data points plotted per complete transducer record

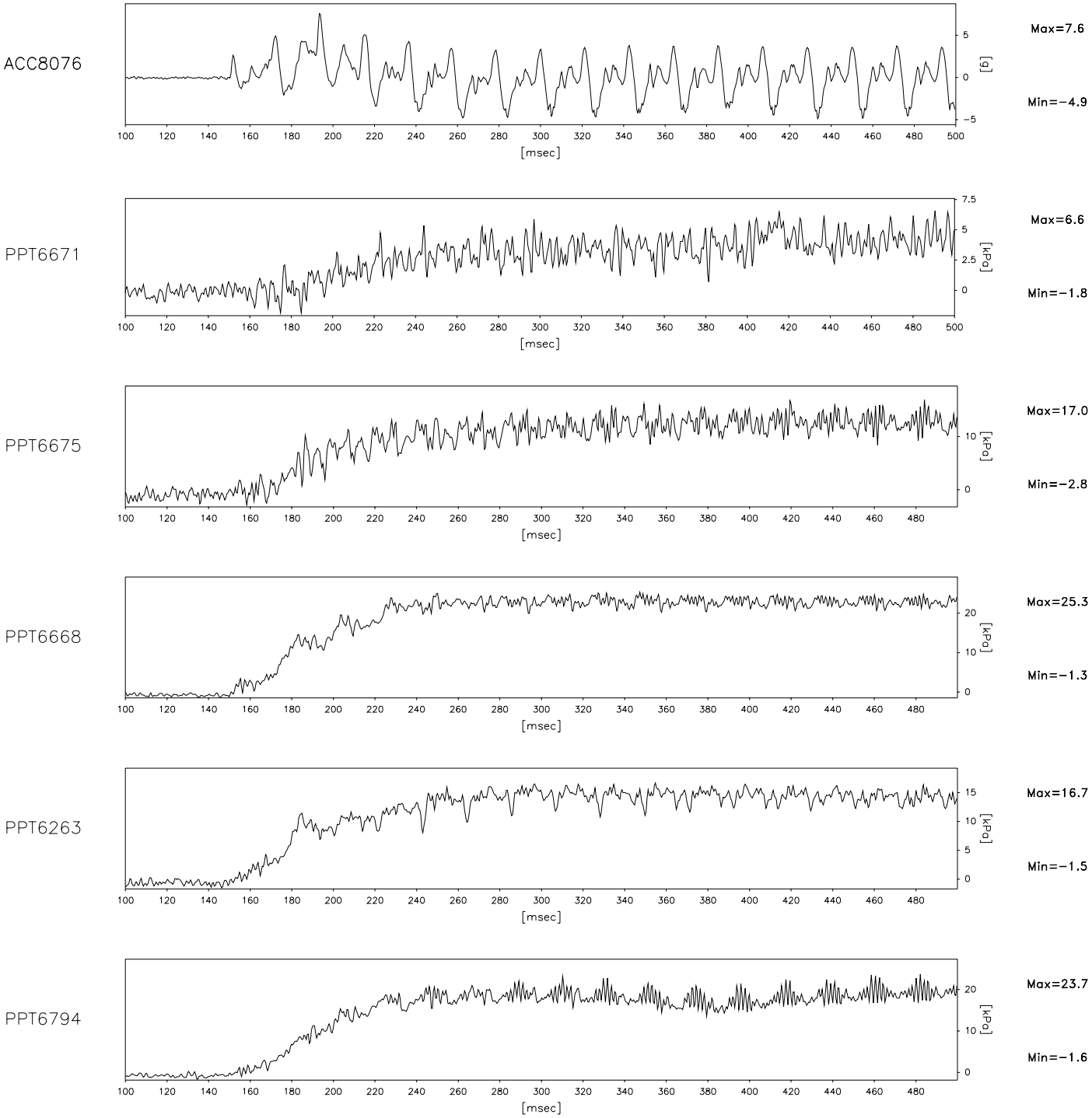

Scales : Model

TEST SKH−5 MODEL 3 deg slope FLIGHT 1		Short−Term TIME RECORDS	Earthquake 1	FIG.NO.

1795 data points plotted per complete transducer record

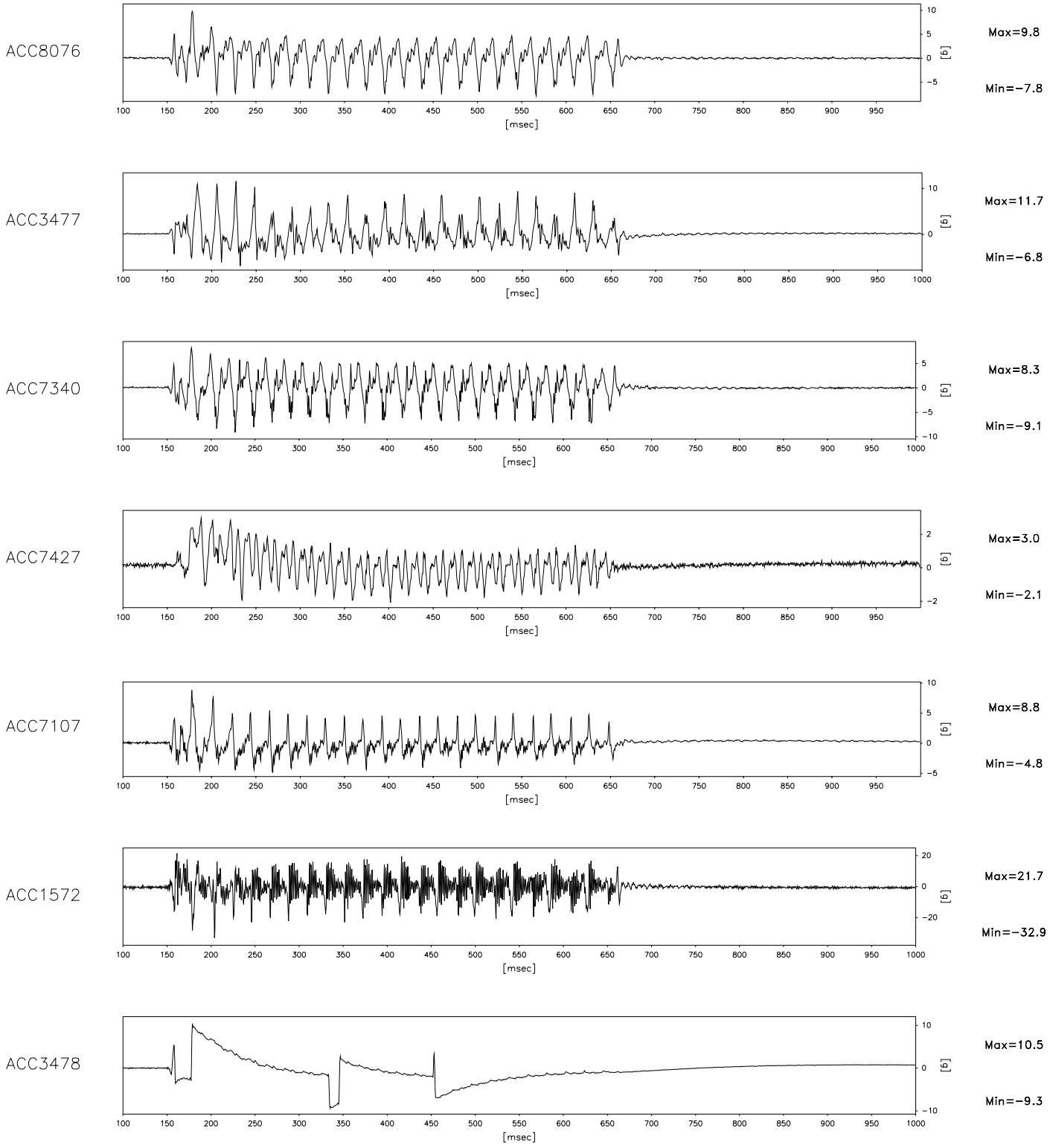

Scales : Model

TEST SKH−5 MODEL 3 deg slope FLIGHT 1		Short−Term TIME RECORDS	Earthquake 2	FIG.NO.

1795 data points plotted per complete transducer record

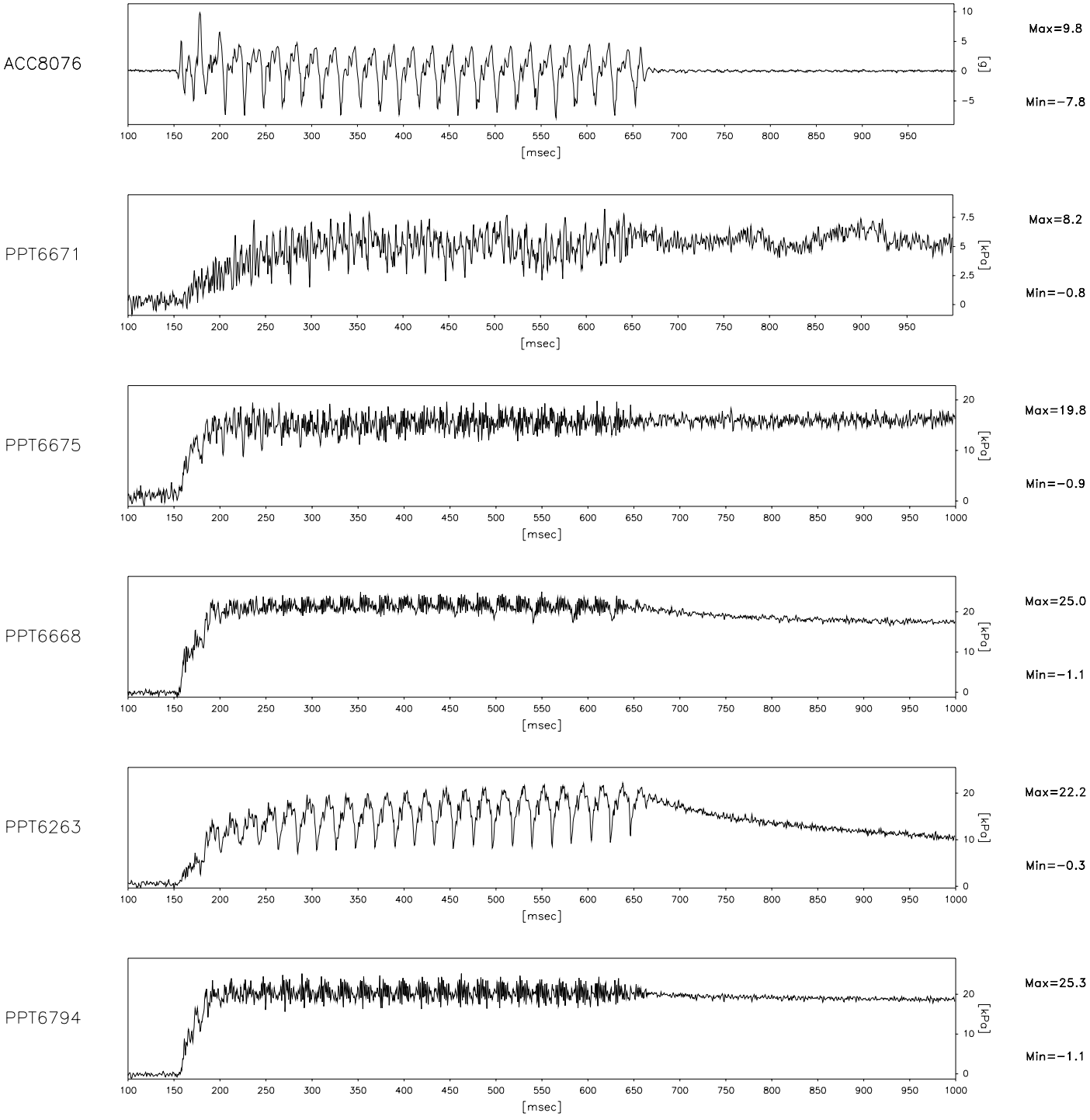

Scales : Model

TEST SKH−5 MODEL 3 deg slope FLIGHT 1		Short−Term TIME RECORDS	Earthquake 2	FIG.NO.

1795 data points plotted per complete transducer record

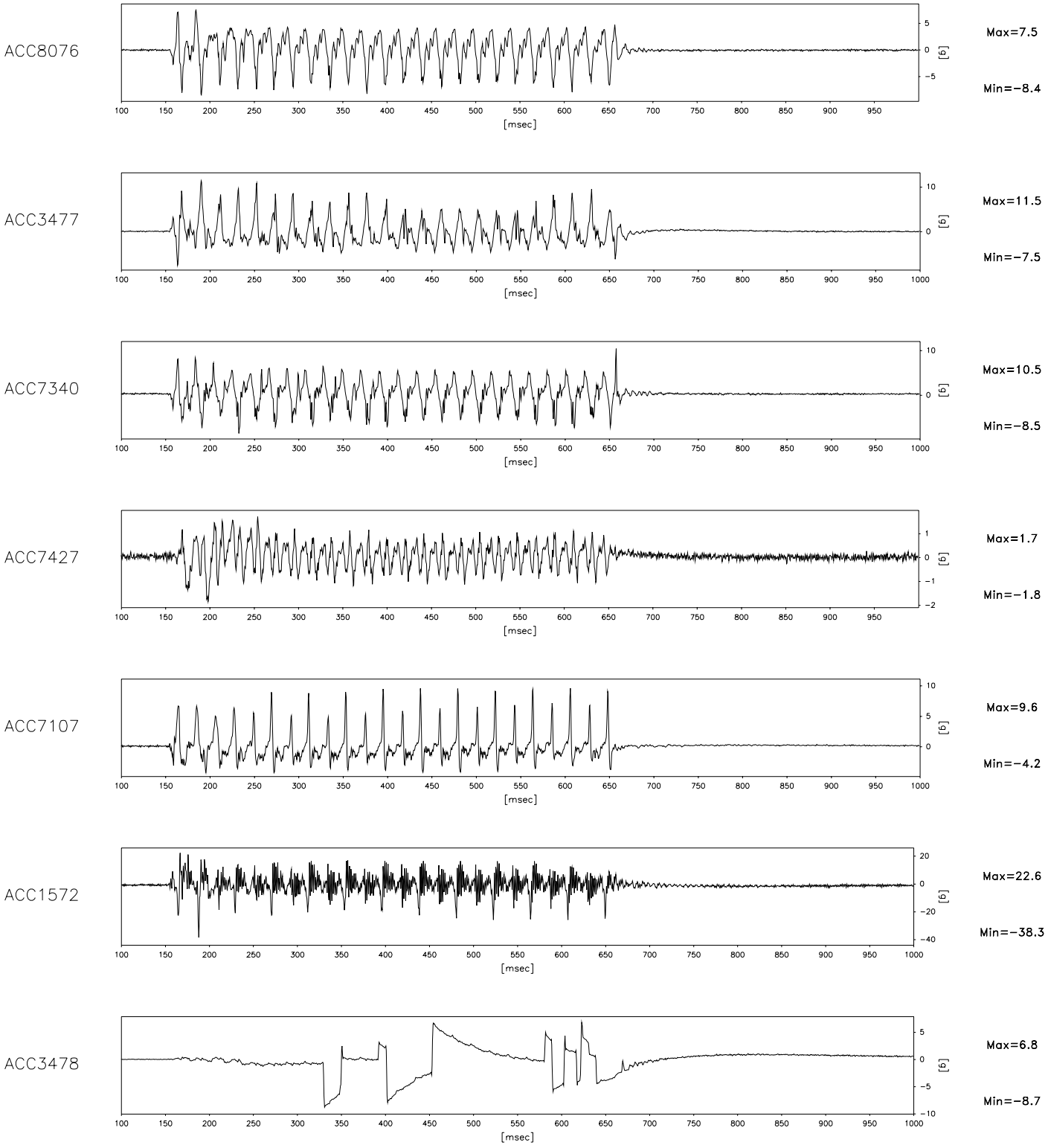

Scales : Model

TEST SKH−5 MODEL 3 deg slope FLIGHT 1		Short−Term TIME RECORDS	Earthquake 3	FIG.NO.

1795 data points plotted per complete transducer record

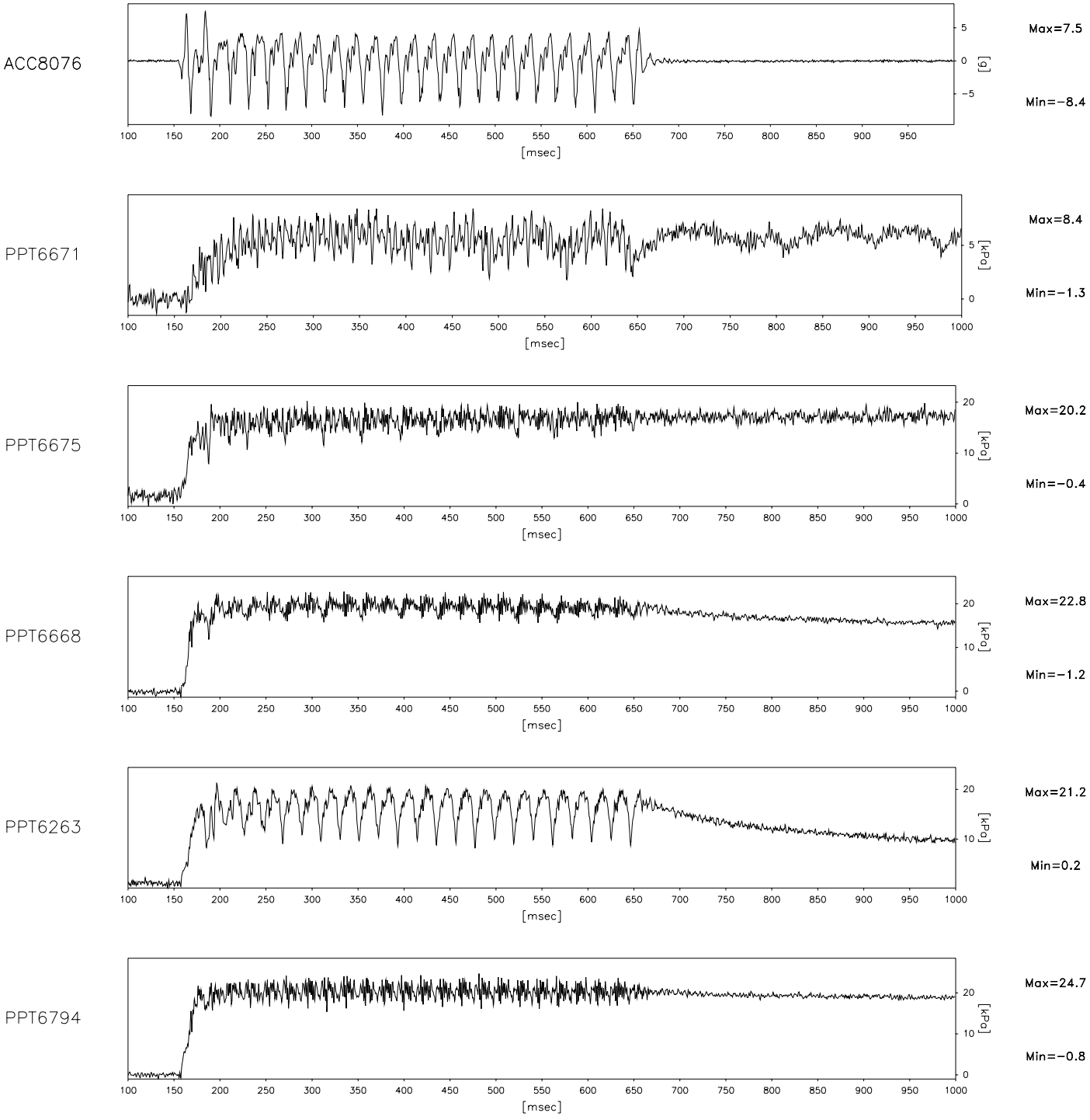

Scales : Model

TEST SKH−5 MODEL 3 deg slope FLIGHT 1		Short−Term TIME RECORDS	Earthquake 3	FIG.NO.

2004 data points plotted per complete transducer record

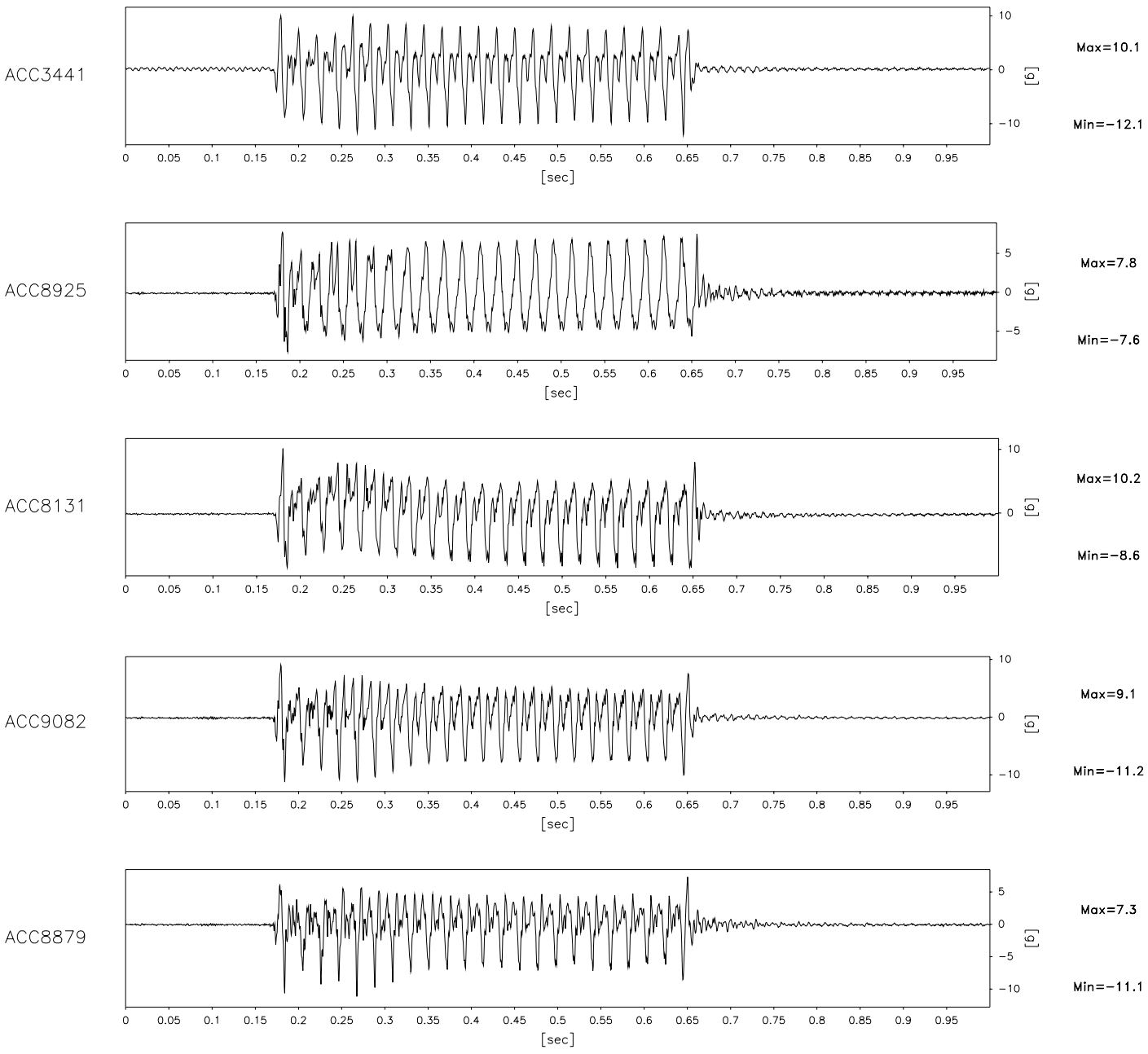

Scales : Model

TEST SKH−8 MODEL 6 deg slope FLIGHT 1		Short−Term TIME RECORDS	Earthquake 1	FIG.NO.

1803 data points plotted per complete transducer record

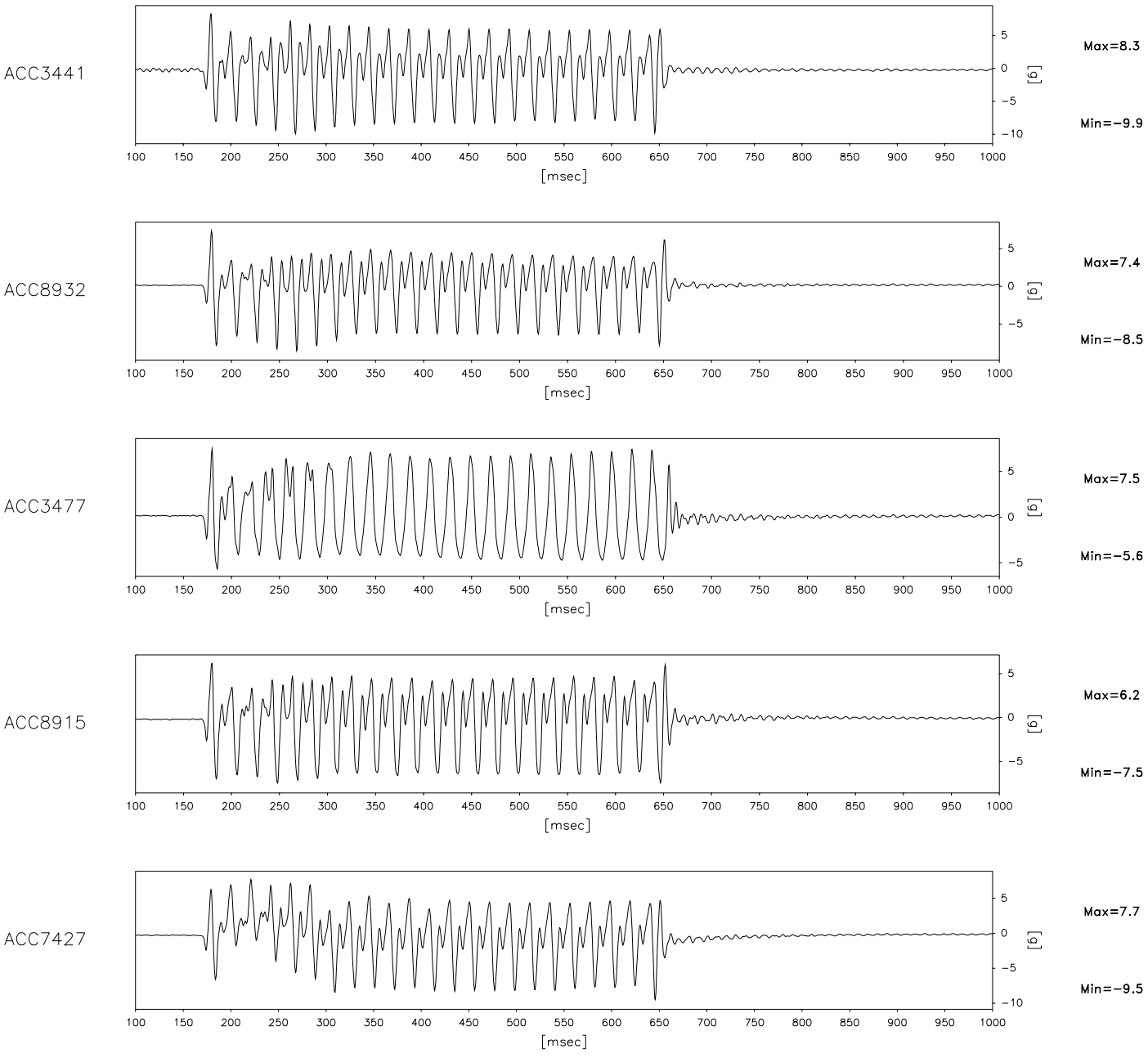

Scales : Model

TEST SKH−8 MODEL 6 deg slope FLIGHT 1		Short−Term TIME RECORDS	Earthquake 1	FIG.NO.

3805 data points plotted per complete transducer record

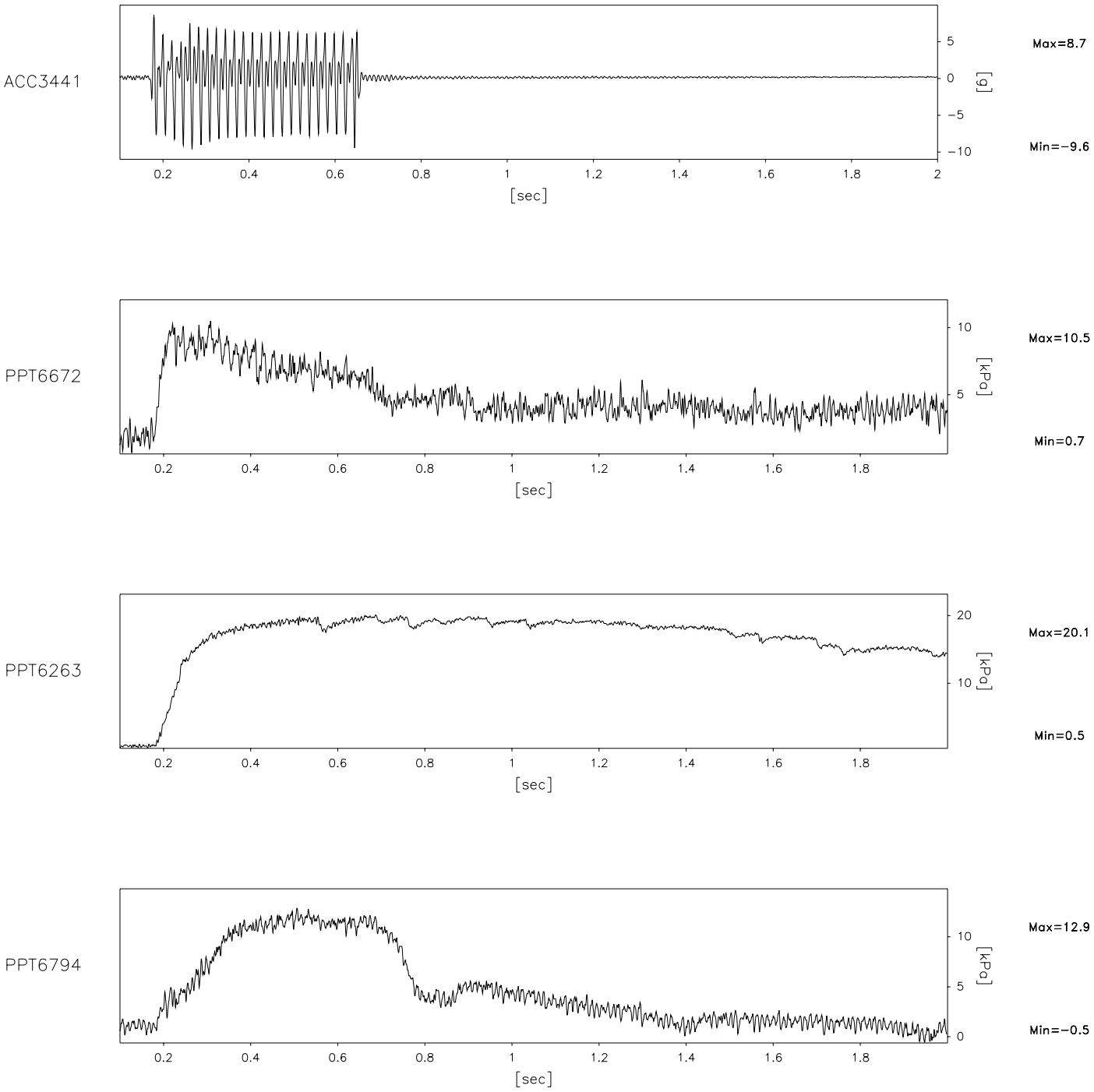

Scales : Model

TEST SKH−8 MODEL 6 deg slope FLIGHT 1		Short−Term TIME RECORDS	Earthquake 1	FIG.NO.

3005 data points plotted per complete transducer record

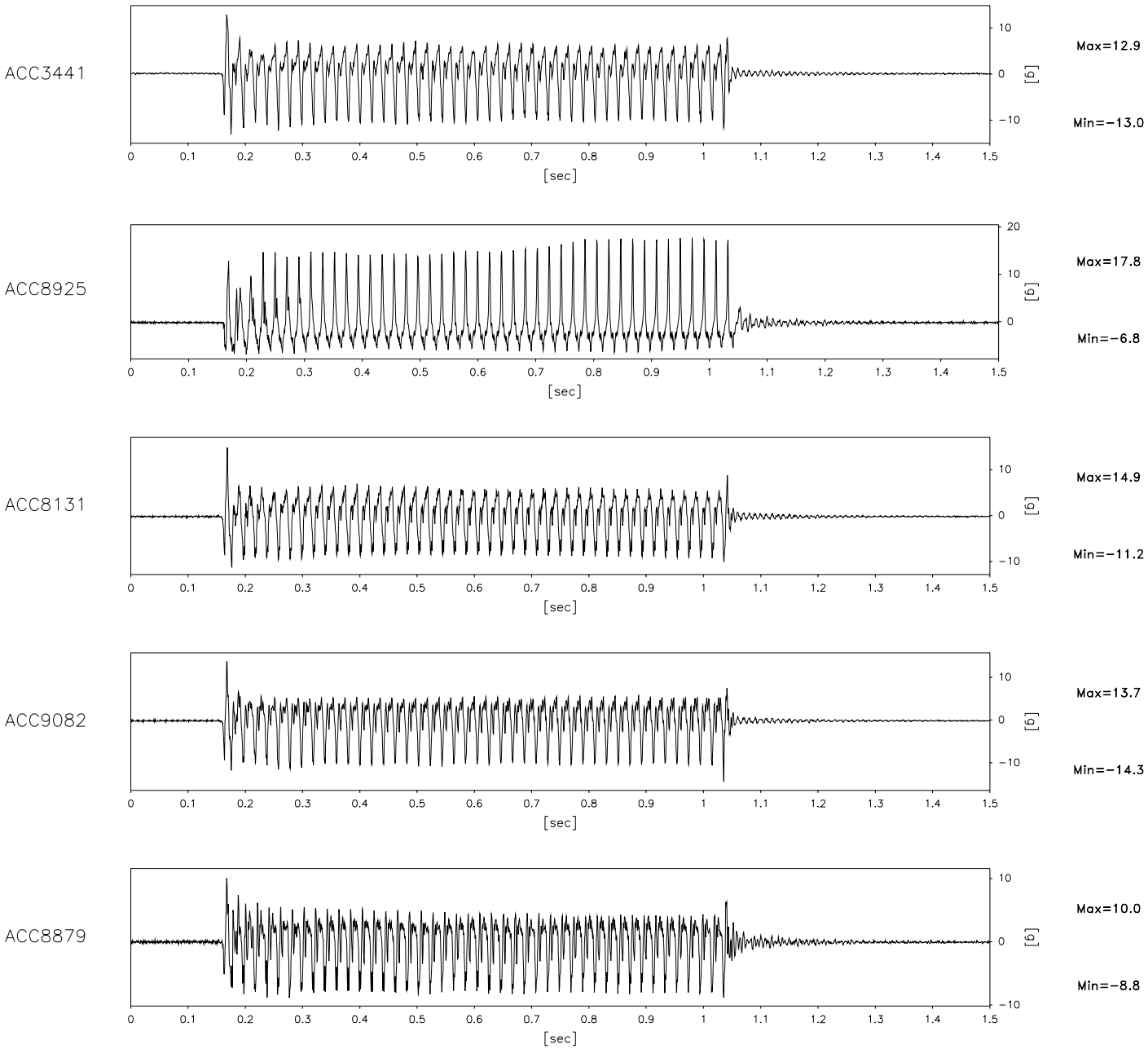

Scales : Model

TEST SKH−8 MODEL 6 deg slope FLIGHT 1		Short−Term TIME RECORDS	Earthquake 2	FIG.NO.

2804 data points plotted per complete transducer record

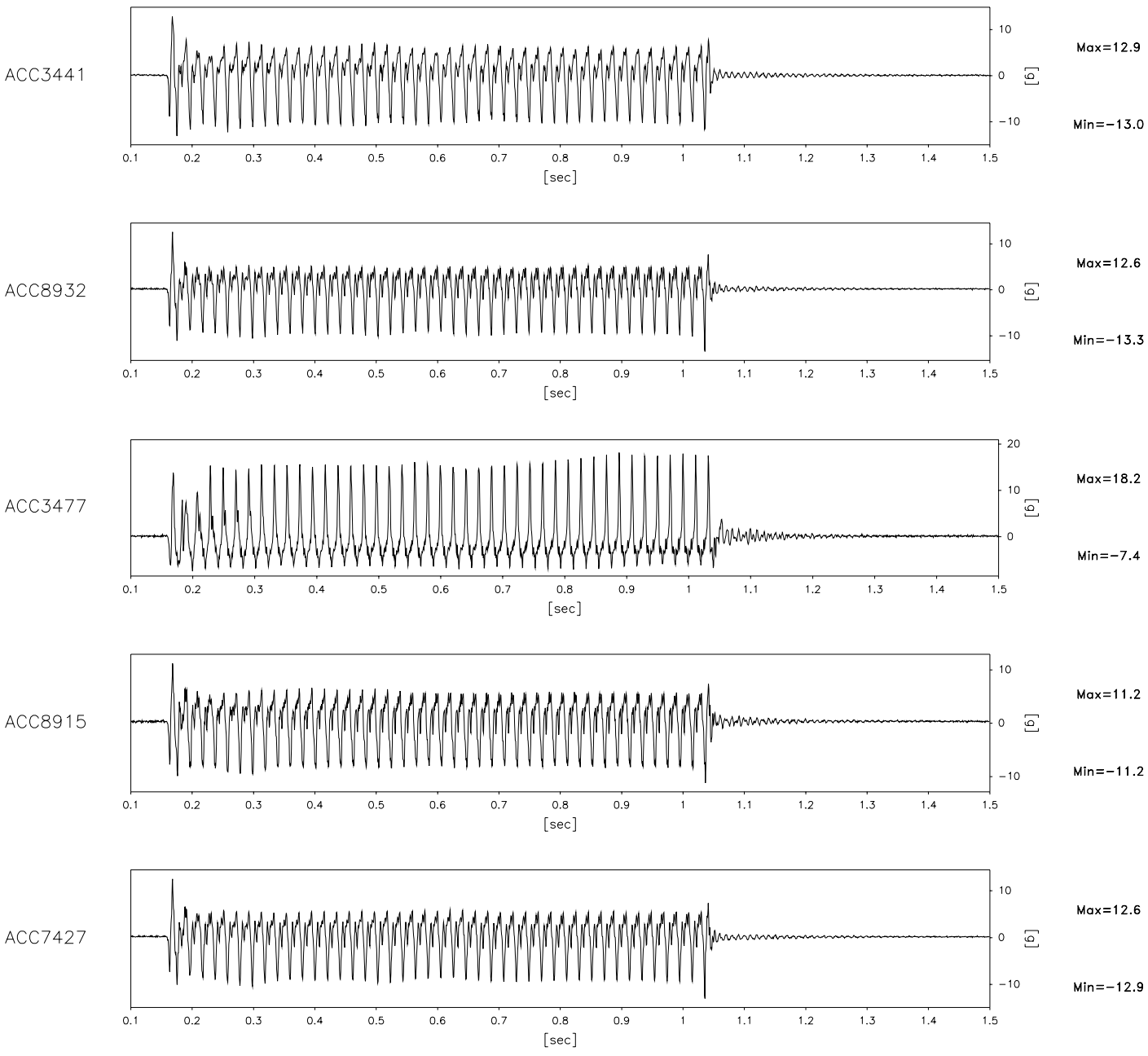

Scales : Model

TEST SKH−8 MODEL 6 deg slope FLIGHT 1		Short−Term TIME RECORDS	Earthquake 2	FIG.NO.

7812 data points plotted per complete transducer record

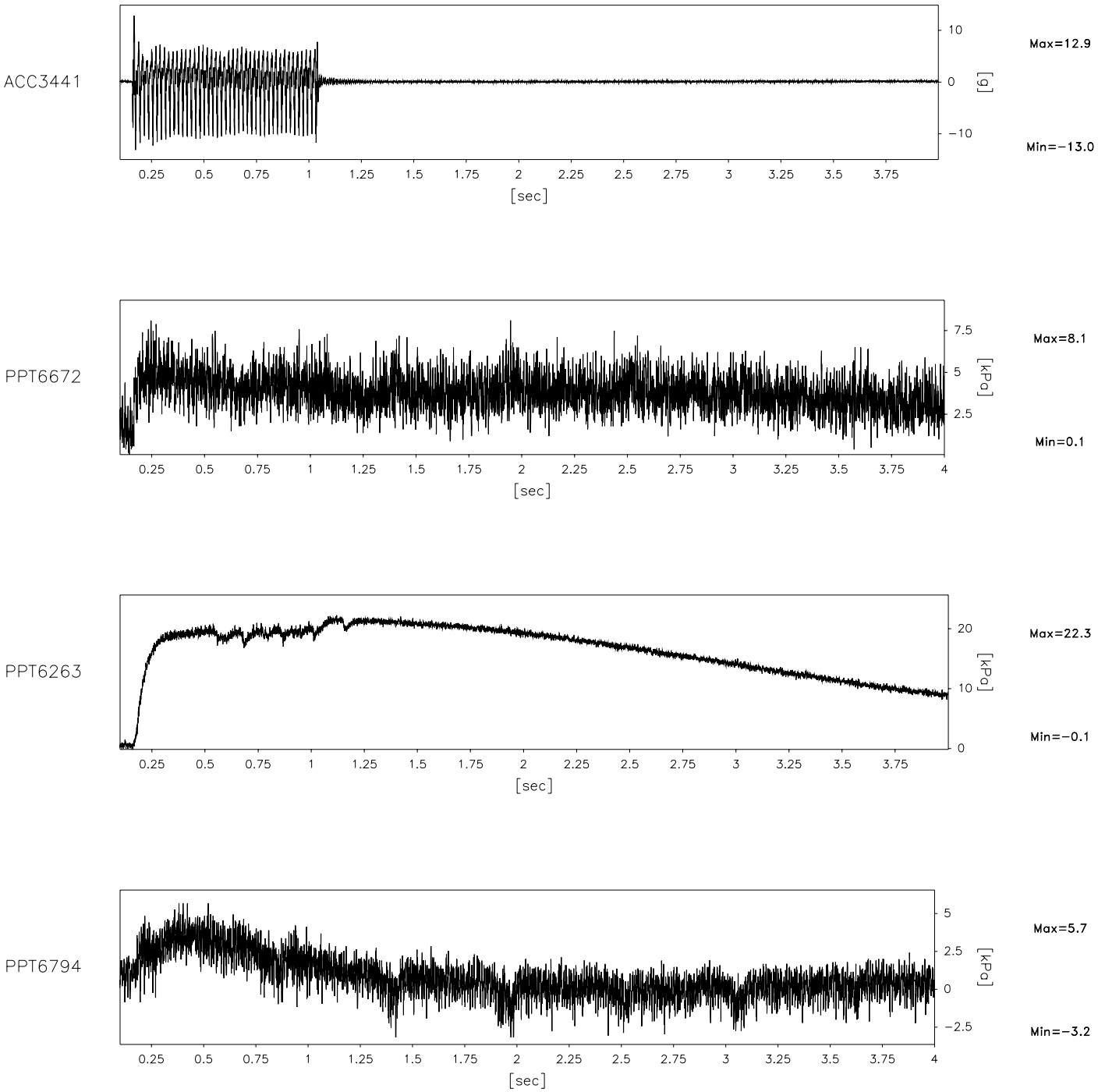

Scales : Model

TEST SKH−8 MODEL 6 deg slope FLIGHT 1		Short−Term TIME RECORDS	Earthquake 2	FIG.NO.

1803 data points plotted per complete transducer record

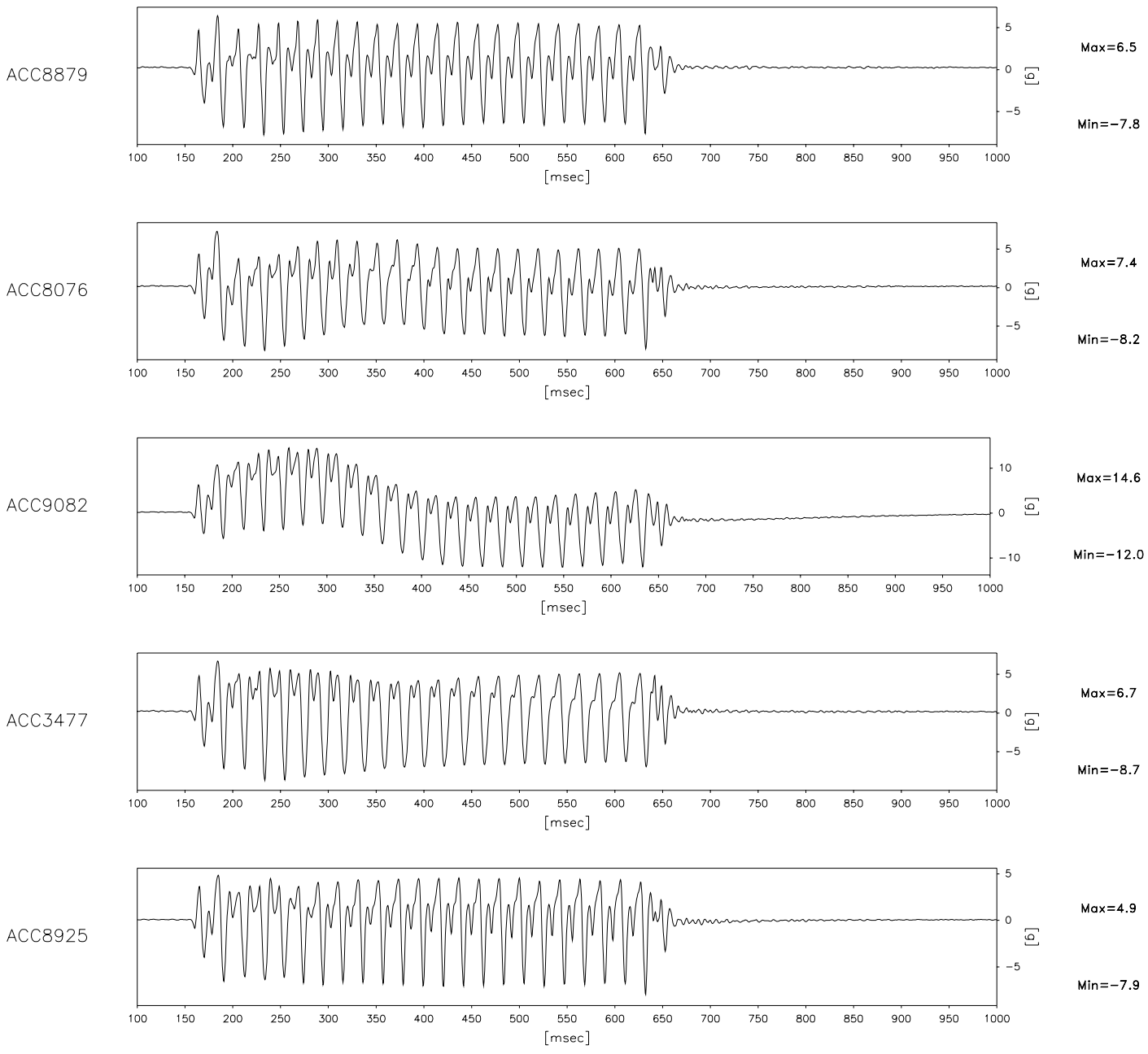

Scales : Model

TEST SKH−9 MODEL 12 deg slope FLIGHT 1		Short−Term TIME RECORDS	Earthquake 1	FIG.NO.

1803 data points plotted per complete transducer record

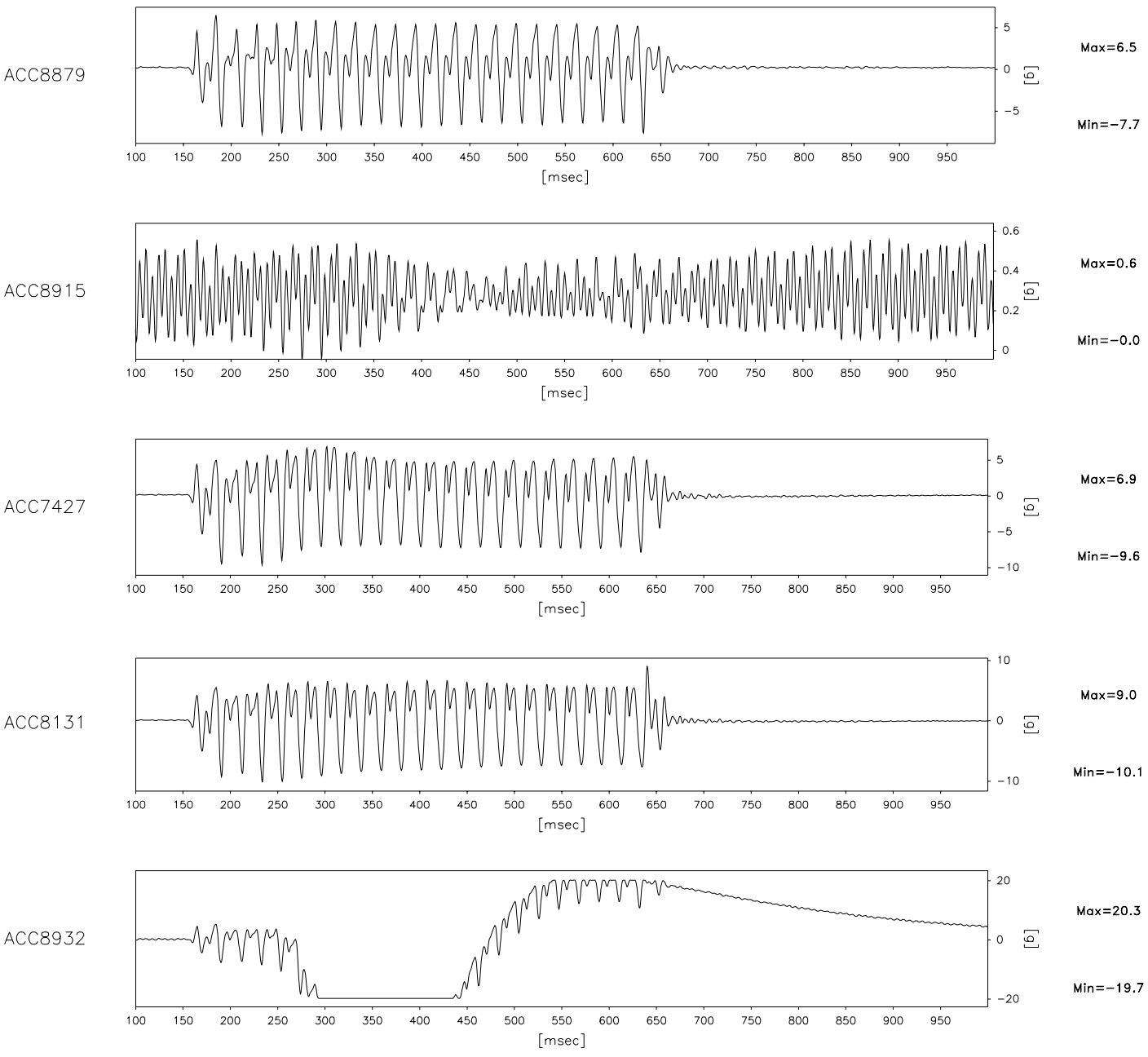

Scales : Model

TEST SKH−9 MODEL 12 deg slope FLIGHT 1		Short−Term TIME RECORDS	Earthquake 1	FIG.NO.

1202 data points plotted per complete transducer record

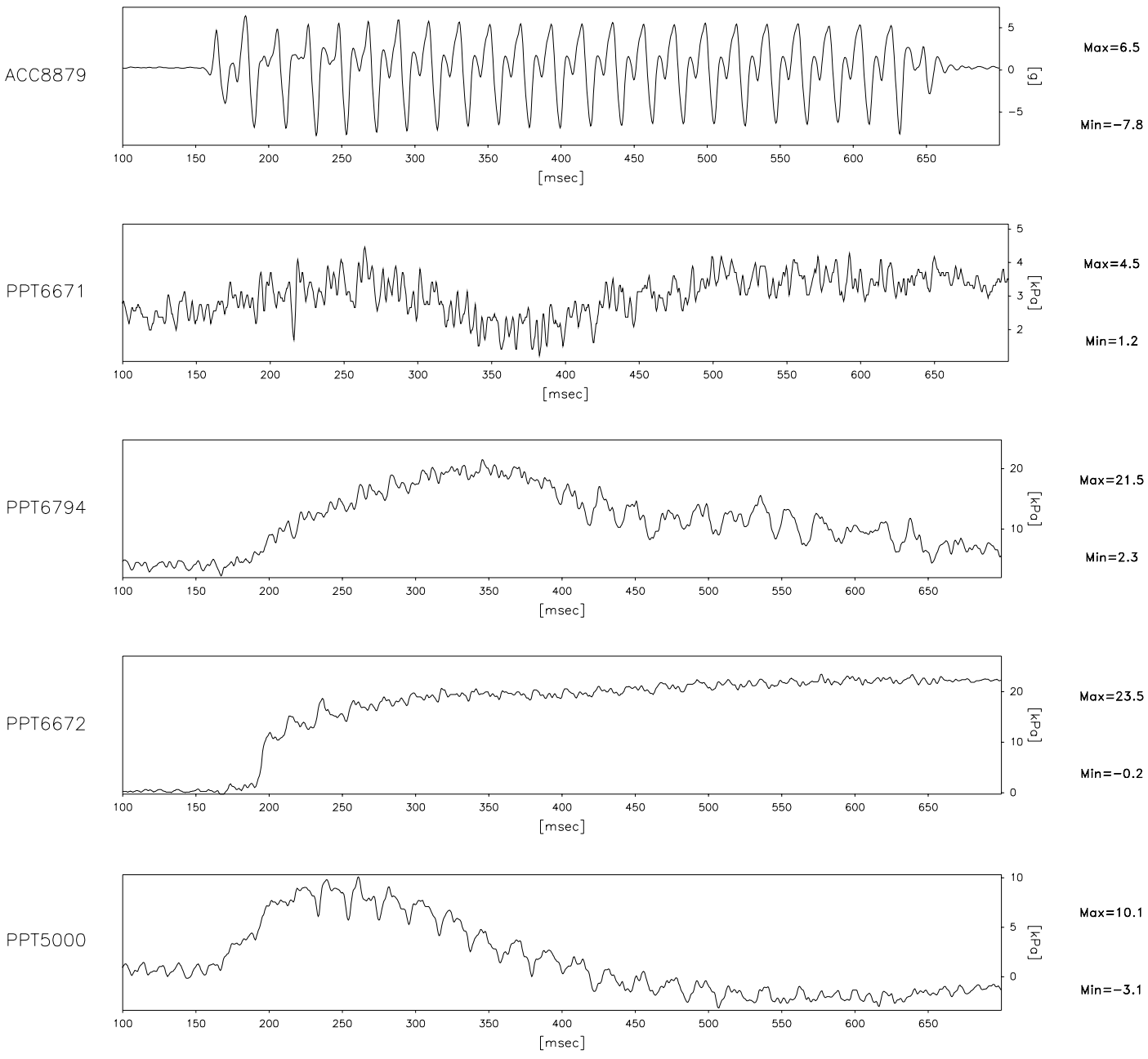

Scales : Model

TEST SKH−9 MODEL 12 deg slope FLIGHT 1		Short−Term TIME RECORDS	Earthquake 1	FIG.NO.

7812 data points plotted per complete transducer record

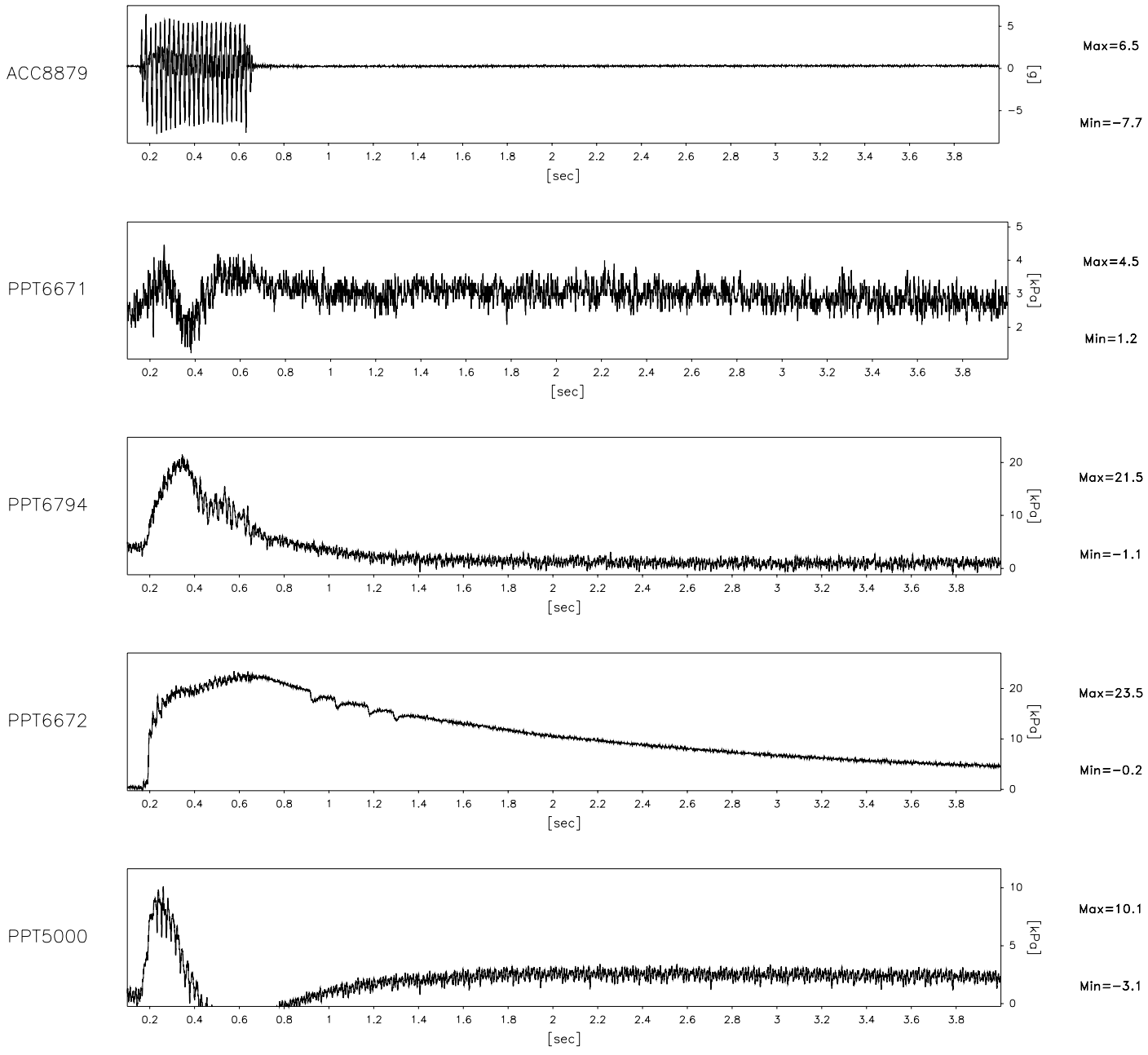

Scales : Model

TEST SKH−9 MODEL 12 deg slope FLIGHT 1		Long−Term TIME RECORDS	Earthquake 1	FIG.NO.

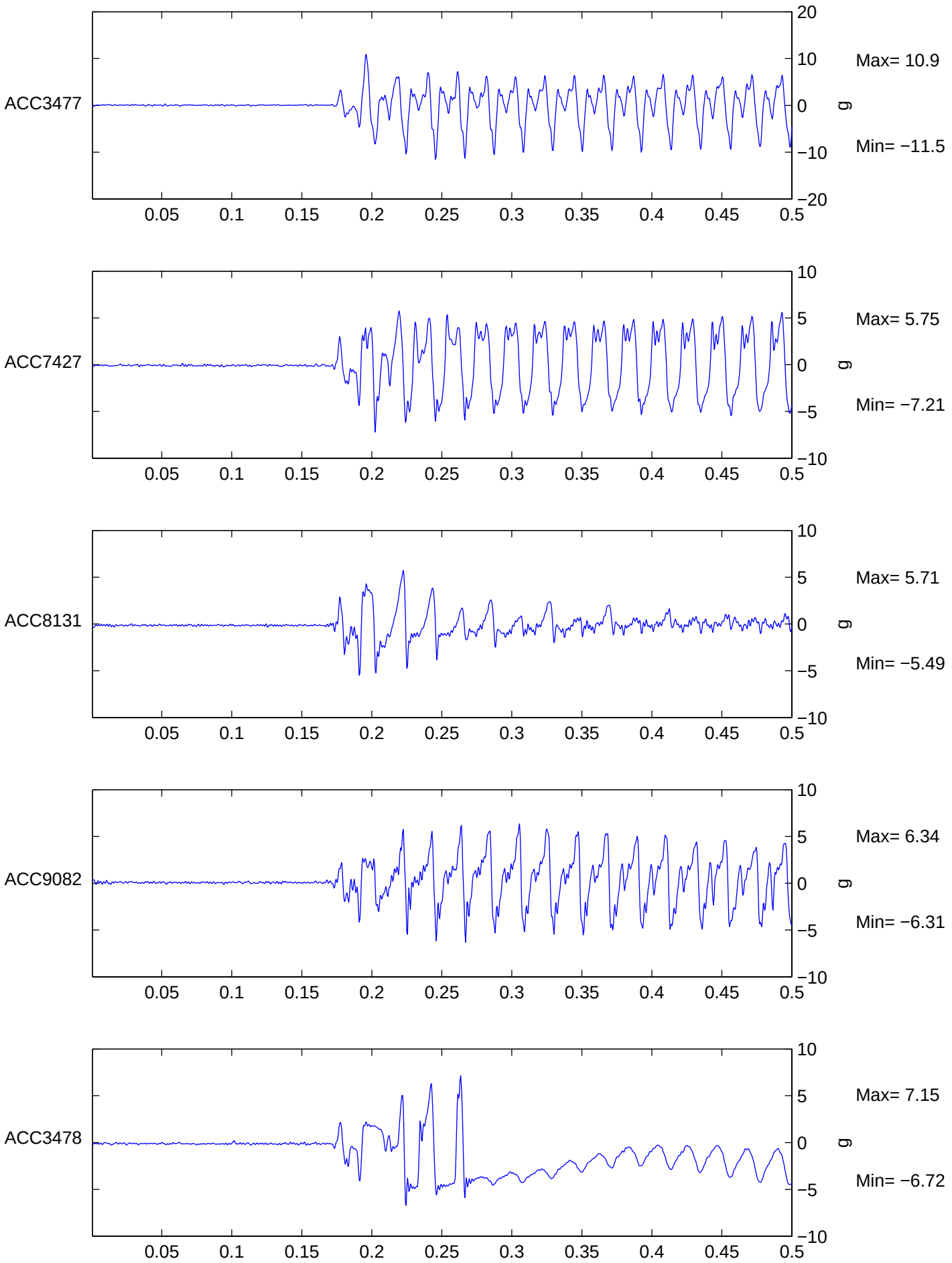

TEST SKH−10 FLIGHT 1		Scales: Model 8th order Butterworth Filter at 500Hz Short−Term Time Records	Earthquake 1	Figure No.

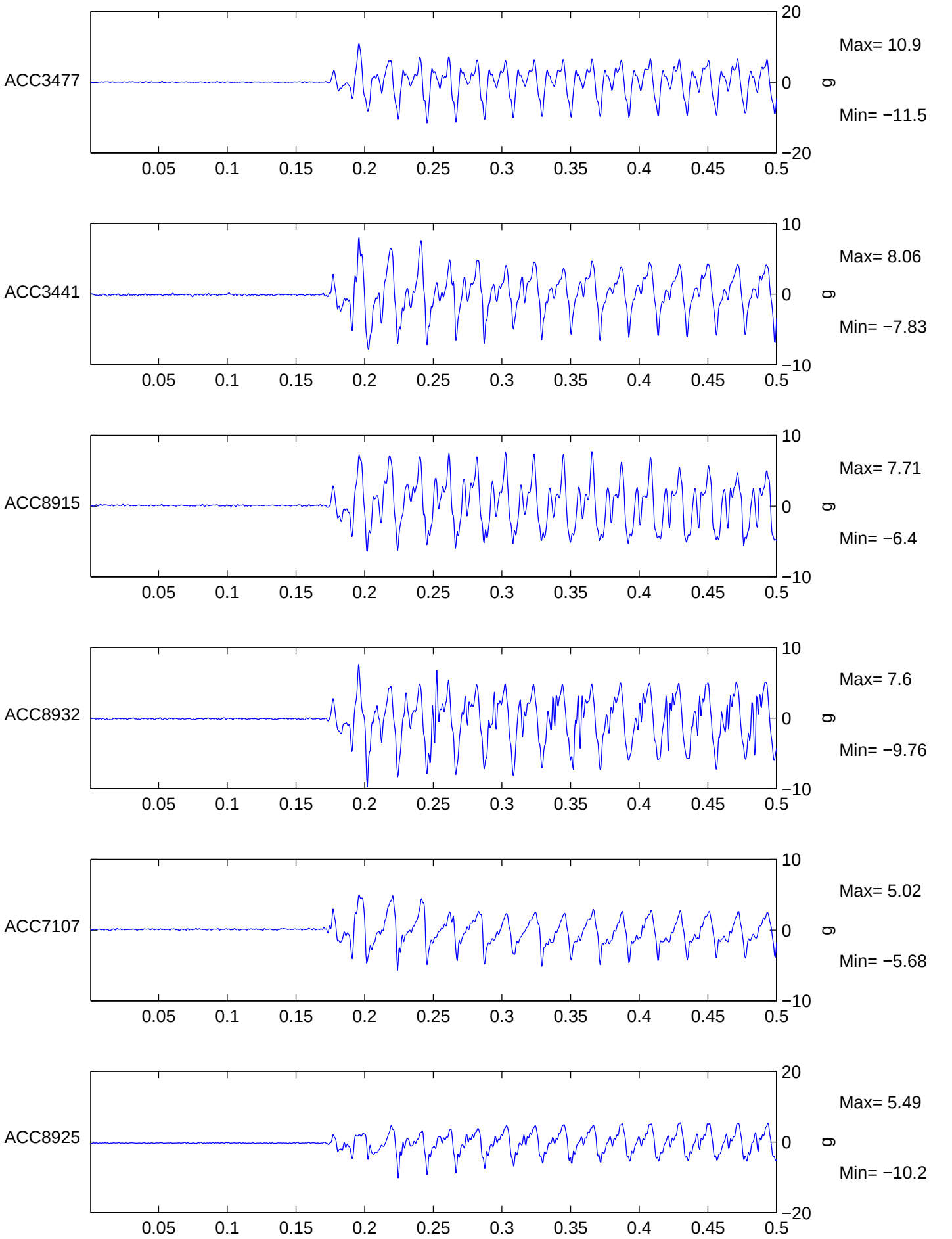

TEST SKH−10 FLIGHT 1		Scales: Model 8th order Butterworth Filter at 500Hz Short−Term Time Records	Earthquake 1	Figure No.

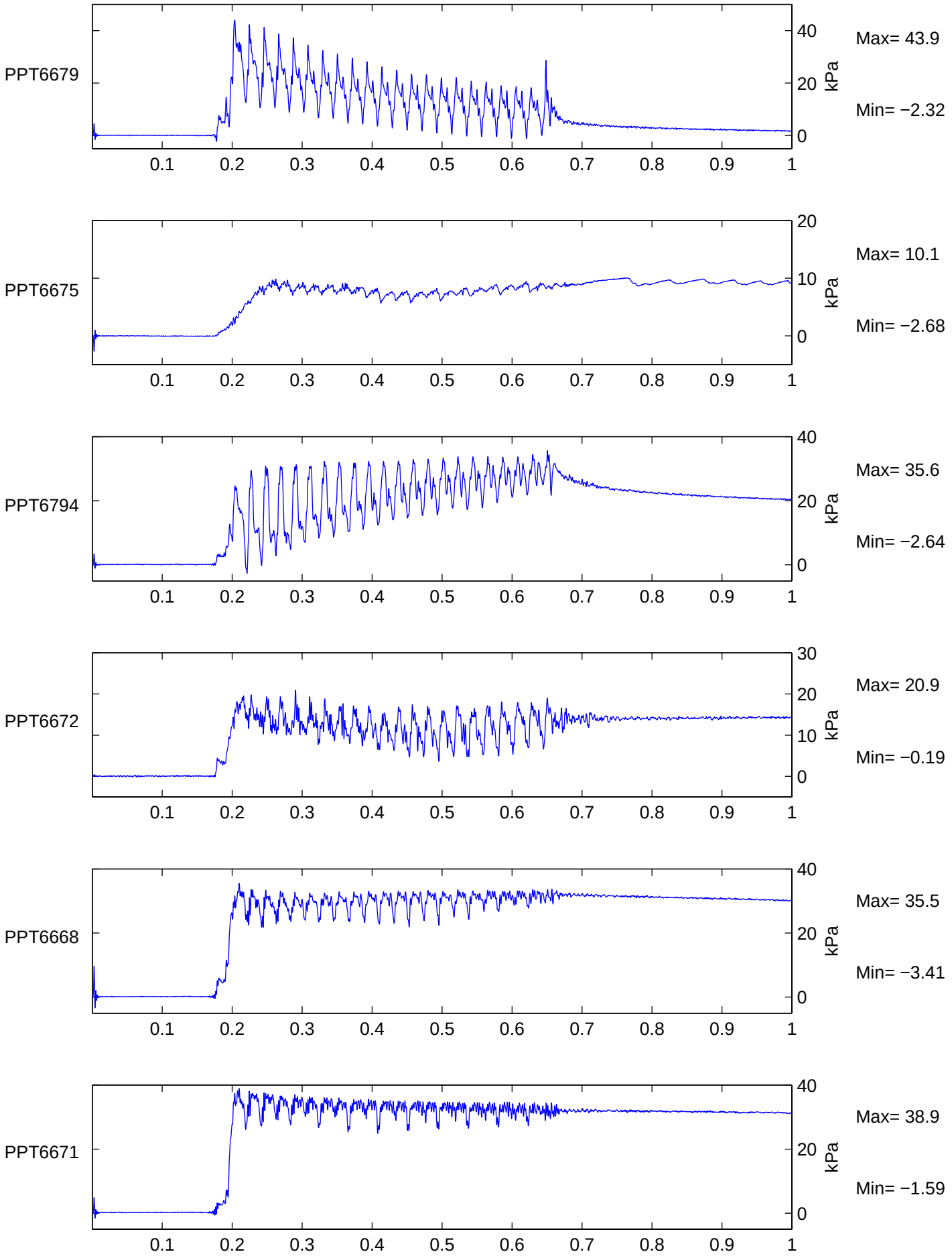

TEST SKH−10 FLIGHT 1		Scales: Model 8th order Butterworth Filter at 500Hz Short−Term Time Records	Earthquake 1	Figure No.

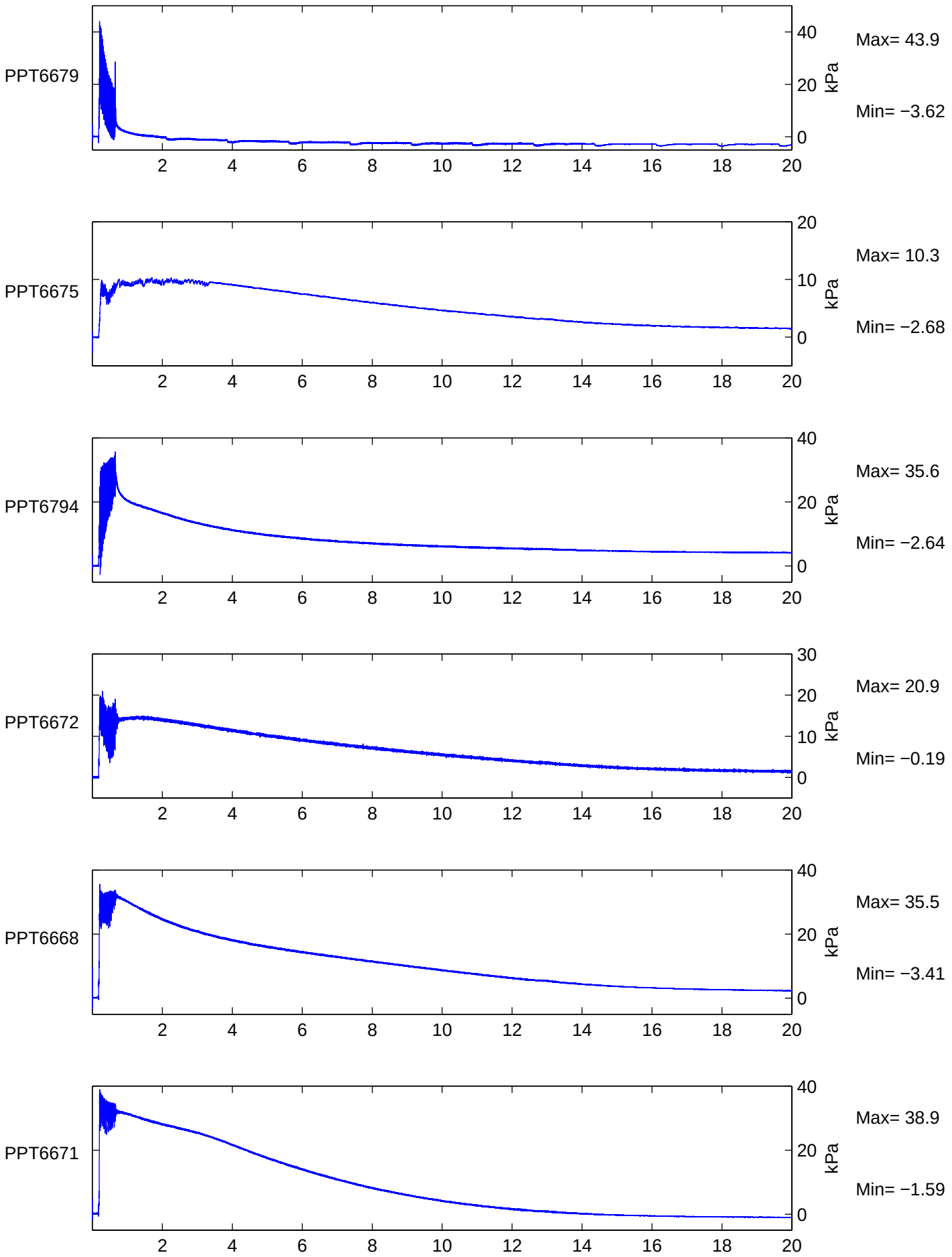

TEST SKH−10 FLIGHT 1		Scales: Model 8th order Butterworth Filter at 500Hz Long−Term Time Records	Earthquake 1	Figure No.

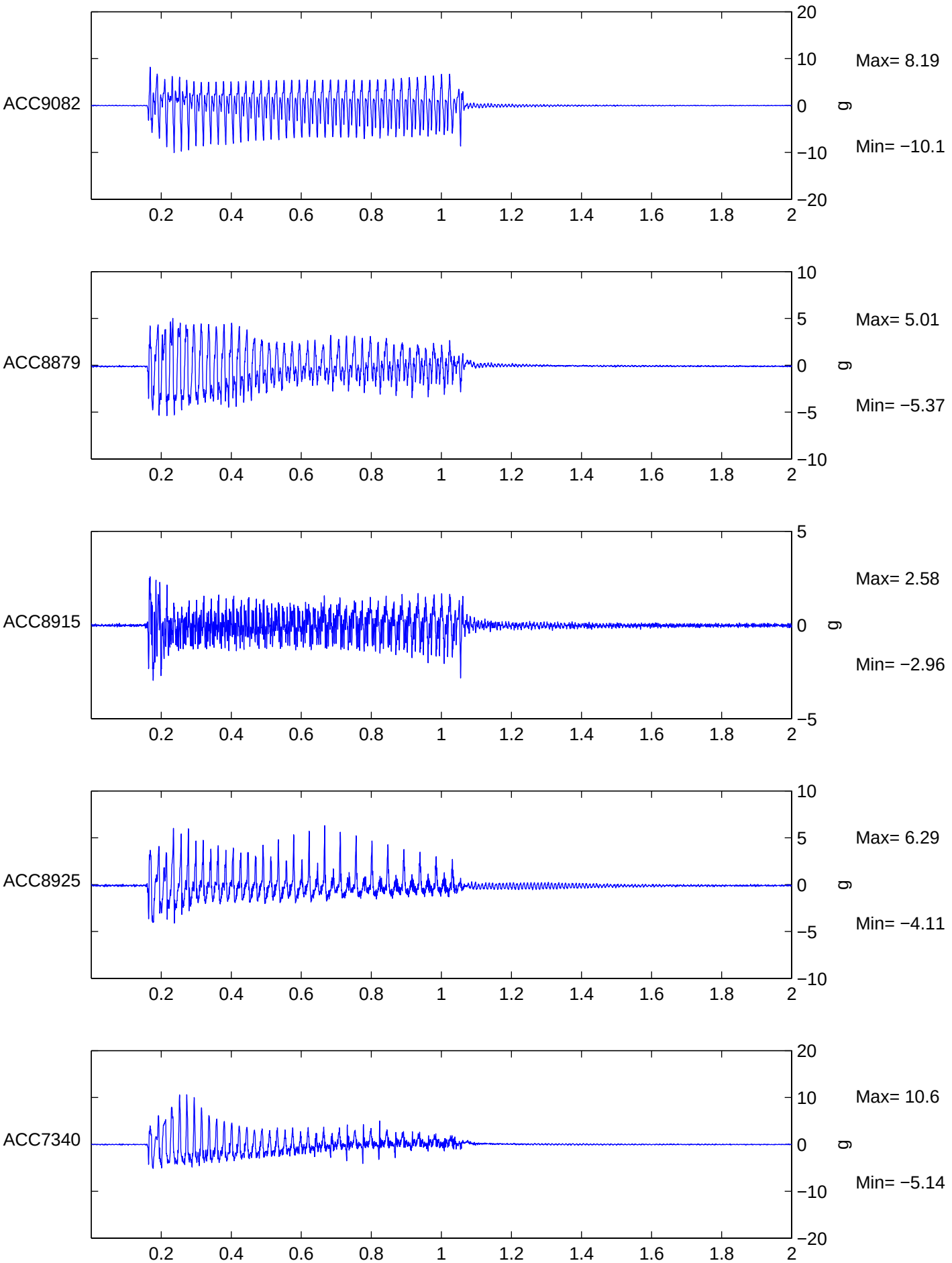

TEST SKH11 FLIGHT 1		Scales: Model 8th order Butterworth Filter at 500Hz Short−Term Time Records	Earthquake 1	Figure No.

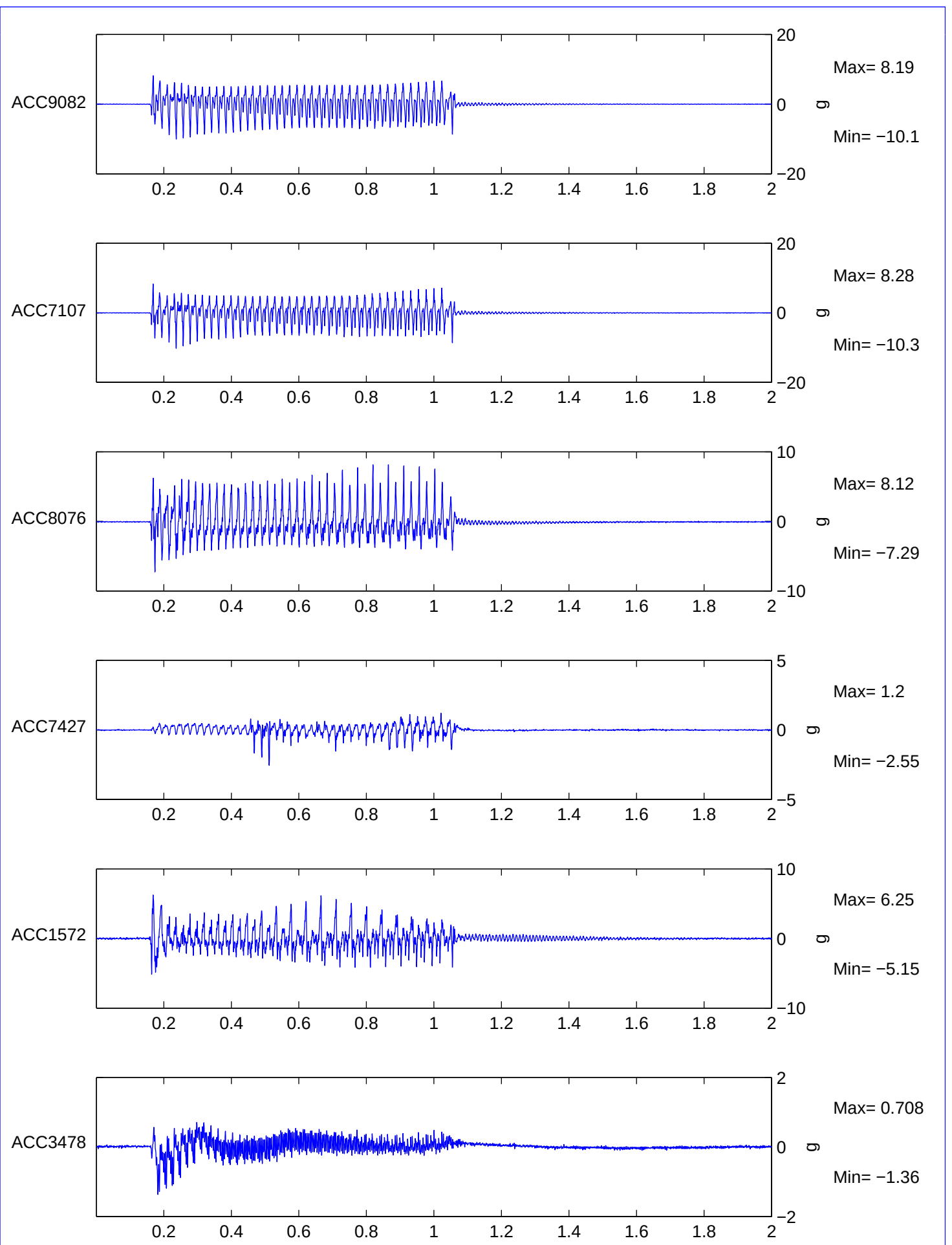

TEST SKH11 FLIGHT 1		Scales: Model 8th order Butterworth Filter at 500Hz Short−Term Time Records	Earthquake 1	Figure No.

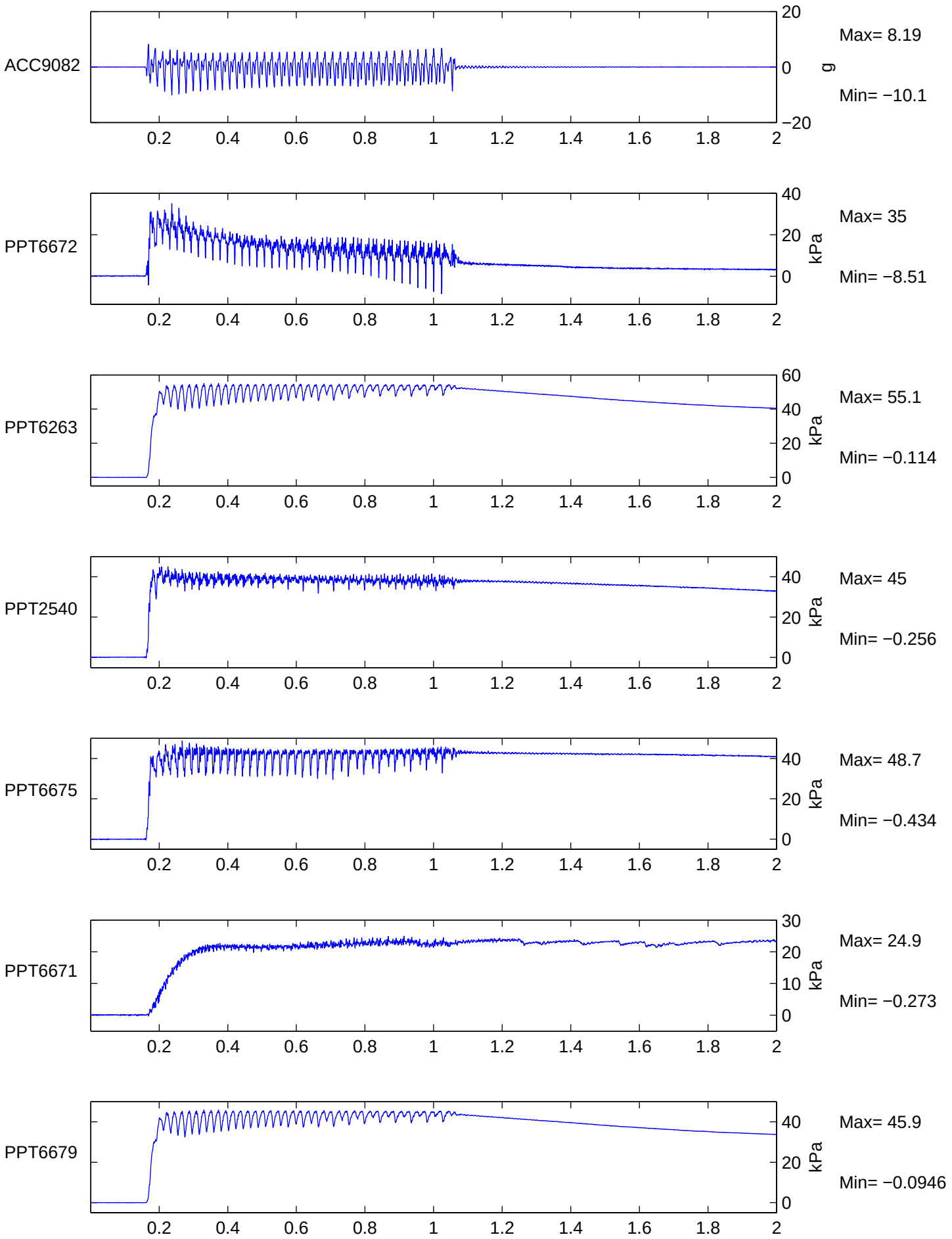

TEST SKH11 FLIGHT 1		Scales: Model 8th order Butterworth Filter at 500Hz Short−Term Time Records	Earthquake 1	Figure No.

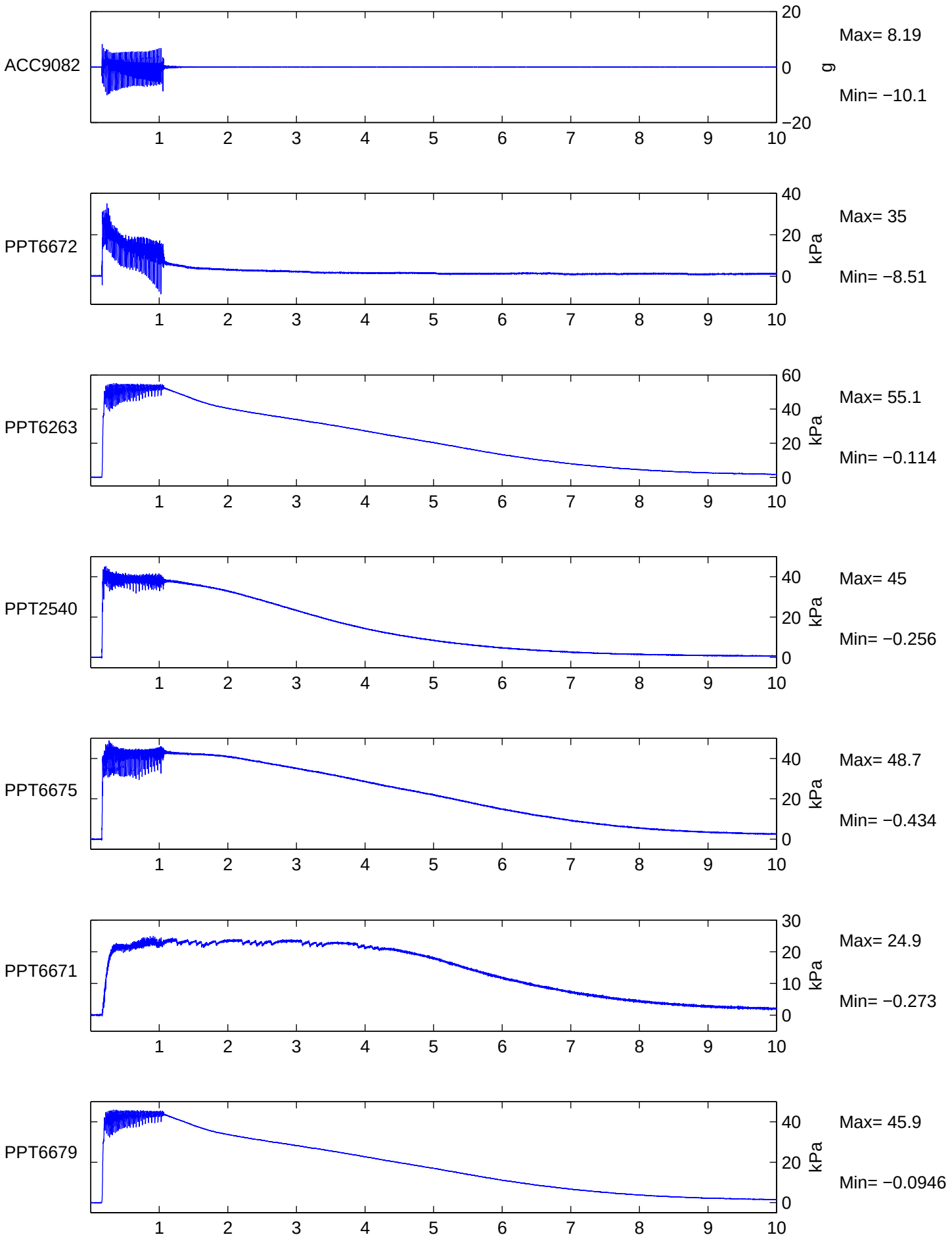

TEST SKH11 FLIGHT 1		Scales: Model 8th order Butterworth Filter at 500Hz Long−Term Time Records	Earthquake 1	Figure No.

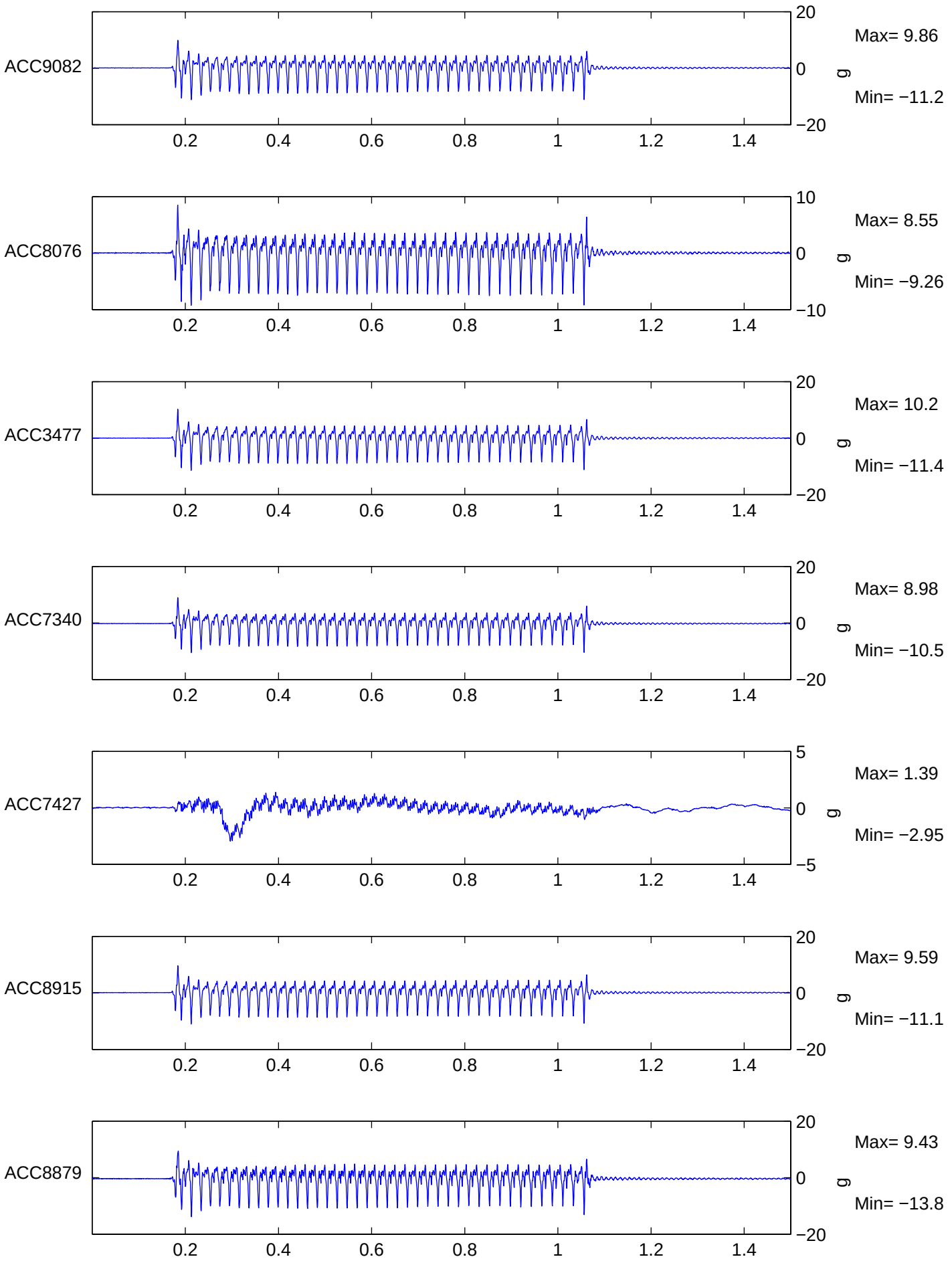

TEST SKH−12 FLIGHT 1		Scales: Model 8th order Butterworth Filter at 500Hz Short−Term Time Records	Earthquake 1	Figure No.

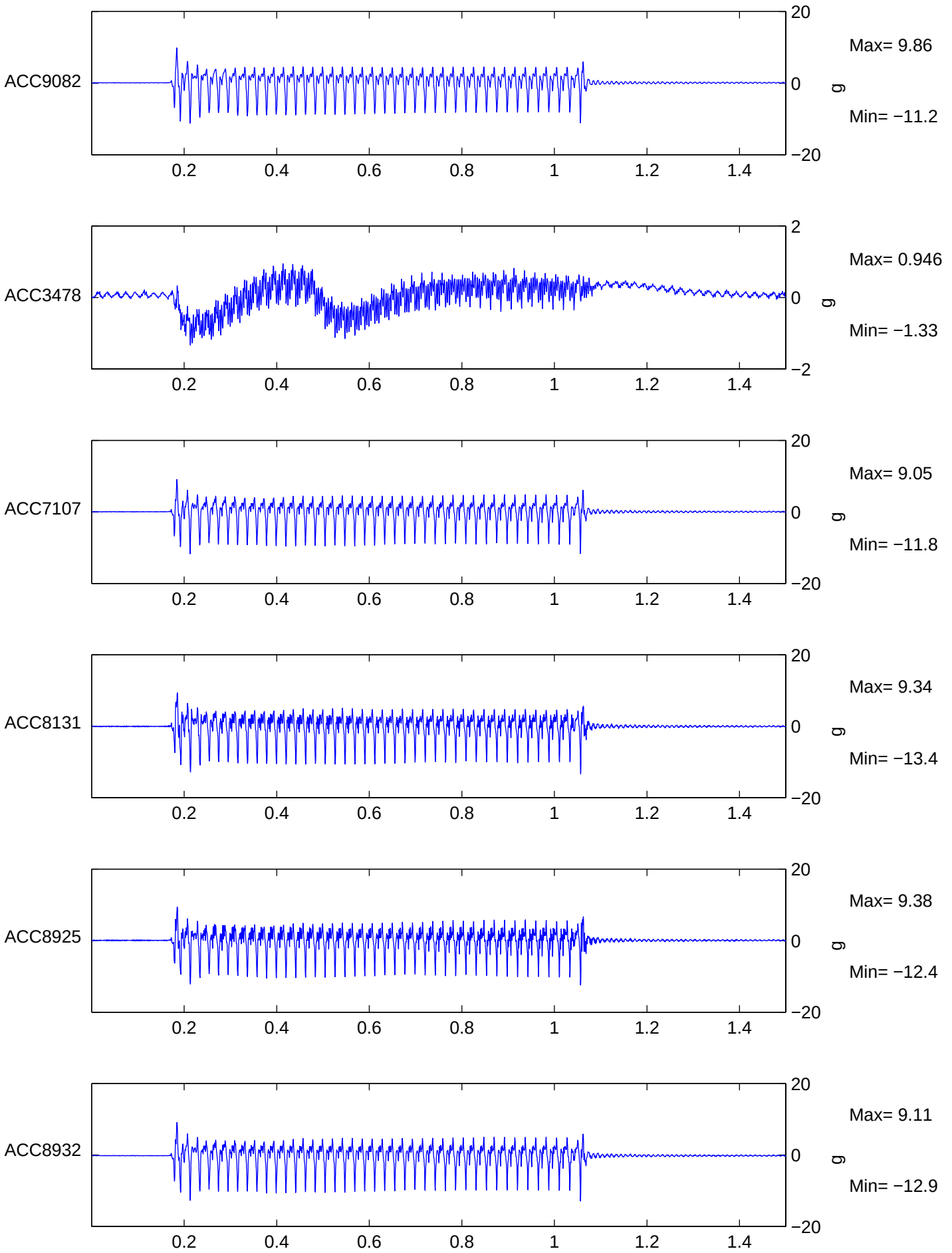

TEST SKH−12 FLIGHT 1		Scales: Model 8th order Butterworth Filter at 500Hz Short−Term Time Records	Earthquake 1	Figure No.

5. Conclusions

It has been shown that centrifuge modelling can be used to investigate the dynamic behaviour of liquefying slopes. Dynamic effects such as resonance and filtering of higher harmonics were observed which are further discussed by Haigh (2002). It was also observed that peak ground surface displacements may not be equal to the greatest displacements occurring within the soil layer.

6. Acknowledgements

The author would like to acknowledge the financial contributions of Shimizu Corporation, Japan, and of the Engineering and Physical Sciences Research Council to this work. The author would also like to acknowledge the contribution of Dr Gopal Madabhushi to this research.

7. References

Haigh, S.K., Madabhushi, S.P.G., Soga, K., Taji, Y. & Shamoto, Y. (2000) "Lateral spreading during centrifuge model earthquakes", Proc. GeoEng2000, Melbourne, Australia

Haigh, S.K. (2002), "Effects of liquefaction-induced lateral spreading on pile foundations in sloping ground", PhD Thesis, Cambridge University, UK

Hamada, M. (1992), "Large ground deformations and their effects on lifelines: 1964 Niigata earthquake", in Case Studies of Liquefaction and Lifeline Performance During Past Earthquakes, Hamada & O'Rourke eds., Technical Report NCEER-92-0001, NCEER, Buffalo, NY

Lee, S.Y. (1990), "Centrifuge modelling of cone penetration testing in cohesionless soils", PhD Thesis, Cambridge University, UK

Tan, F.S.C. (1990), "Centrifuge and theoretical modelling of conical footings on sand", PhD Thesis, Cambridge University, UK